Published in final edited form as:

Nature. 2016 May 19; 533(7603): 411–415. doi:10.1038/nature17662.

An obligatory role for neurotensin in high fat diet-induced obesity

J. Li[1,2], **J. Song**[*,1,2], **Y.Y. Zaytseva**[*,1,2], **Y. Liu**[2], **P. Rychahou**[1,2], **K. Jiang**[2], **M.E. Starr**[1,2], **J. T. Kim**[1,2], **J.W. Harris**[1,2], **F.B. Yiannikouris**[3,4], **W.S. Katz**[3], **P.M. Nilsson**[5,6], **M. Orho-Melander**[5], **J. Chen**[7,8], **H. Zhu**[7,8], **T. Fahrenholz**[4], **R.M. Higashi**[2,4], **T. Gao**[2,7], **A.J. Morris**[9], **L.A. Cassis**[3], **T.W-M. Fan**[2,4], **H.L. Weiss**[2,10], **P. R. Dobner**[11], **O. Melander**[5,6], **J. Jia**[†,2,7], and **B.M. Evers**[†,1,2]

[1]Department of Surgery, University of Kentucky, Lexington, KY

[2]Markey Cancer Center, University of Kentucky, Lexington, KY

[3]Department of Pharmacology and Nutritional Sciences, University of Kentucky, Lexington, KY

[4]Graduate Center for Toxicology and Center for Environmental and Systems Biochemistry, University of Kentucky, Lexington, KY

[5]Department of Clinical Sciences, Lund University, Malmö, Sweden

[6]Department of Internal Medicine, Skåne University Hospital, Malmö, Sweden

[7]Department of Molecular and Cellular Biochemistry, University of Kentucky, Lexington, KY

[8]Center for Structural Biology, University of Kentucky, Lexington, KY

[9]Division of Cardiovascular Medicine, Gill Heart Institute, University of Kentucky and Lexington Veterans Affairs Medical Center, Lexington, KY

[10]Department of Biostatistics, University of Kentucky, Lexington, KY

[11]Department of Microbiology and Physiological Systems, University of Massachusetts Medical School, Worcester, MA

Abstract

Corresponding Author: B. Mark Evers, MD, University of Kentucky, Markey Cancer Center, CC140 Roach Building, Lexington, KY 40536, Tel: (859) 323-6556, Fax: (859) 323-2074, mark.evers@uky.edu.

*These authors contributed equally to this work

†Senior authors

Correspondence and requests for materials should be addressed to mark.evers@uky.edu.

Author Contributions

J.L., J.J., P.R.D., O.M. and B.M.E. designed the research; J.L., J.S., Y.Y.Z., Y.L., P.R. and K.J. performed experiments; J.T.K. assisted with experiments; M.E.S. and J.W.H. assisted with the animal work; W.S.K., F.B.Y. and L.A.C. performed indirect metabolism and adipocyte size analyses; J.C. and H.Z. designed and performed the proteomics studies using LC-MS/MS for NT analysis of the *Drosophila* samples; A.J.M. performed LC-MS analysis; T.W-M.F. and R.M.H. designed ^{13}C-OA tracer study, reviewed the manuscript, and together with T.F. performed FT-MS data analyses; H.L.W. performed statistical analyses; P.R.D. provided NT KO mice and reviewed the manuscript; T.G. reviewed the manuscript and provided comments and suggestions; P.M.N., M.O-M. and O.M. performed and analyzed human studies; J.L., J.J., H.L.W. and B.M.E. reviewed and interpreted data; J.L., J.J., P.R.D. and B.M.E. wrote the manuscript.

The authors declare no competing financial interests.

Obesity and its associated comorbidities (e.g., diabetes mellitus and hepatic steatosis) contribute to approximately 2.5 million deaths annually[1] and are among the most prevalent and challenging conditions confronting the medical profession[2,3]. Neurotensin (NT), a 13-amino acid peptide predominantly localized in specialized enteroendocrine (EE) cells of the small bowel[4] and released by fat ingestion[5], facilitates fatty acid (FA) translocation in rat intestine[6], and stimulates growth of various cancers[7]; the effects of NT are mediated through three known NT receptors (NTR1, 2 and 3)[8]. Increased fasting plasma levels of pro-NT (a stable NT precursor fragment produced in equimolar amounts relative to NT) are associated with increased risk of diabetes, cardiovascular disease and mortality[9]; however, a role for NT as a causative factor in these diseases is unknown. Here, we show that NT-deficient mice demonstrate significantly reduced intestinal fat absorption and are protected from obesity, hepatic steatosis and insulin resistance associated with high fat consumption. We further demonstrate that NT attenuates the activation of AMP-activated protein kinase (AMPK) and stimulates FA absorption in mice and in cultured intestinal cells, and that this occurs through a mechanism involving NTR1 and NTR3/sortilin. Consistent with the findings in mice, expression of NT in *Drosophila* midgut EE cells results in increased lipid accumulation in the midgut, fat body, and oenocytes (specialized hepatocyte-like cells) and decreased AMPK activation. Remarkably, in humans, we show that both obese and insulin-resistant subjects have elevated plasma concentrations of pro-NT, and in longitudinal studies among non-obese subjects, high levels of pro-NT denote a doubling of the risk of developing obesity later in life. Our findings directly link NT with increased fat absorption and obesity and suggest that NT may provide a prognostic marker of future obesity and a potential target for prevention and treatment.

Keywords

gut hormone; obesity; hepatic steatosis; insulin resistance; AMPK

To examine the potential role of NT in fat deposition and obesity, we initially compared NT-deficient mice[10,11] to wild type littermates fed a standard diet (18% kcal from fat) for 6 months. Average body length, small bowel weight and length, villus height and crypt number did not differ between genotypes (Extended Data Fig. 1a–f). However, the epididymal and retroperitoneal fat pads of $NT^{-/-}$ mice were consistently smaller as compared to wild type (Extended Data Fig. 2a–c). Indeed, when challenged with a high-fat diet (HFD; 60% kcal from fat), epididymal, retroperitoneal, and pericardiac fat deposits were markedly smaller in $NT^{-/-}$ mice (Extended Data Fig. 2d–f). Moreover, body weight was significantly less in both male and female $NT^{-/-}$ mice fed HFD (Fig. 1a–b) and male $NT^{-/-}$ mice fed a low-fat diet (LFD; 10% kcal from fat) (Extended Data Fig. 2g) compared with wild type. No differences in body weight were noted between female $NT^{+/+}$ and $NT^{-/-}$ mice fed LFD (Extended Data Fig. 2g). EchoMRI assessment of total fat (corrected for body weight) further confirmed reduced body fat composition in male $NT^{-/-}$ mice (Extended Data Fig. 2h).

Obesity-associated insulin resistance was also attenuated in NT-deficient mice. On a HFD, NT-deficient mice demonstrated lower levels of fasting plasma glucose and insulin (Fig. 1c), greater insulin sensitivity and faster glucose clearance (Fig. 1d) compared with wild type. Consistently, insulin-stimulated p-Akt expression was decreased in the livers of $NT^{+/+}$ mice

fed HFD, whereas $NT^{-/-}$ mice fed the same diet demonstrated a similar induction of p-Akt following injection of insulin as noted for both wild type and NT-deficient mice fed LFD (Extended Data Fig. 2i). In contrast, there was no difference in insulin secretion comparing $NT^{+/+}$ and $NT^{-/-}$ mice maintained on a normal chow diet following either glucose administration by gavage or refeeding after a 16h fast (Extended Data Fig. 2j,k). Hepatic steatosis (Fig. 1e), liver triglyceride (TG) and cholesterol accumulation (Fig. 1f) were significantly decreased in $NT^{-/-}$ mice fed a HFD. Adipocytes in epididymal fat pads of $NT^{-/-}$ mice showed a reduction in size (Fig. 1g, h) and decreased inflammatory infiltrates and numbers of macrophages (F4/80-positive cells) (Extended Data Fig. 2l,m). Together, these results indicate that NT deficiency protects against comorbidities (i.e., increased insulin resistance and hepatic steatosis) associated with high dietary fat intake.

NT has been linked to hypothalamic leptin signaling[12] and is considered an anorectic peptide based on acute suppression of food intake in rats following intracerebral or intraperitoneal (i.p.) administration of NT[13,14]. When considering total food intake over 22 weeks, there were no differences between genotypes in either male or female mice fed with LFD or males fed a HFD; however, a slight 10% decrease in female $NT^{-/-}$ mice fed a HFD reached significance (Extended Data Fig. 3a). Weekly food consumption was not statistically different in male or female mice fed with LFD or males fed with HFD (Extended Data Fig. 3b, c); only week 9 comparison in females fed HFD reached significance (Extended Data Fig. 3c). Energy expenditure, locomotor activity, energy intake, and respiratory exchange ratios were not different between $NT^{+/+}$ and $NT^{-/-}$ mice fed either HFD or LFD (Extended Data Fig. 3d–g). Although we cannot completely dismiss a potential effect of NT deficiency on feeding behavior, this factor alone does not appear to play a major role in the lower weight gain observed in $NT^{-/-}$ mice fed a HFD.

We next evaluated differences in intestinal lipid absorption as a possible mechanism for the decreased weight gain noted in NT-deficient mice. Compared to $NT^{+/+}$ mice, fecal TG content was increased by ~25% in $NT^{-/-}$ mice fed HFD (Fig. 2a), but was not associated with a change in stool color, consistency or output (Extended Data Fig. 4a), indicating that NT deficiency decreases lipid absorption without overt signs of fat malabsorption (i.e., steatorrhea). Consistently, less and smaller lipid droplets were noted in the mucosa of the proximal intestine of $NT^{-/-}$ mice at 30 and 60min after olive oil gavage compared with $NT^{+/+}$ mice (Fig. 2b). To better track and quantify intestinal absorption, $^{13}C_{18}$-oleic acid ($^{13}C_{18}$-OA) was administered by gavage and measured in the proximal intestine and plasma by Fourier transform-mass spectrometry (FT-MS). $^{13}C_{18}$-OA was significantly decreased in the intestine and at 2 and 3h in plasma of $NT^{-/-}$ mice (Fig. 2c). NT administration (3600 nmol/kg body weight, i.p.)[14] restored TG accumulation in $NT^{-/-}$ mice to levels similar to those in $NT^{+/+}$ mice (Fig. 2d). Similarly, pretreatment of C57BL/6 mice with SR 48692 (2.5mg/kg, ip), a selective nonpeptide NTR1 antagonist that acts peripherally and centrally when administered either ip or by gavage[15], decreased intestinal FA absorption following olive oil gavage (Fig. 2e). To further demonstrate that the effect of SR 48692 was due to disruption of NT signaling, we repeated the experiment using $NT^{-/-}$ mice and their wild type littermates and found that, similar to our initial results, pretreatment with SR 48692 inhibited intestinal FA absorption in wild type mice (as measured by TG accumulation); however, SR pretreatment in $NT^{-/-}$ mice did not further decrease lipid absorption after olive

oil administration which, as expected, was significantly decreased compared to wild type mice (Extended Data Fig. 4b). These results indicate that SR 48692 attenuation of fat uptake reflects the disruption of normal NT signaling and is not due to an unanticipated off-target effect. NT treatment also increased FA uptake in rat intestinal epithelial-1 (RIE-1) cells (Extended Data Fig. 4c, d) that express NTR1 and 3 [similar to human intestinal cells (FHs 74 Int) and mouse intestinal mucosa (Extended Data Fig. 4e–g), and siRNA knockdown of either NTR1 or NTR3, which have been demonstrated to heterodimerize on the cell surface and to broaden the response range for NT signaling[15], reduced NT-mediated FA absorption (Extended Data Fig. 4h, i). Consistent with a role for NT in HFD-induced weight gain, treatment with SR 48692 (2.5mg/kg, oral gavage, twice a day) for 13 weeks significantly attenuated body weight gain in wild type mice fed a HFD (Fig. 2f) without altering food intake (Extended Data Fig. 4j). Collectively, these results indicate that NT promotes intestinal lipid uptake through NTR1 and possibly NTR3 promoting weight gain in mice fed a HFD. Interestingly, Rabinowich et al.[16] recently demonstrated that NTR3/sortilin deficient mice, when placed on a HFD, exhibited a similar phenotype as NT-deficient mice, thus further emphasizing the potential importance of the NT/NTR axis in weight gain associated with an overabundance of fat.

AMPK, a key fuel-sensing enzyme and a critical regulator of metabolism, mediates the effects of a variety of hormones[17,18]. Phosphorylated-AMPK (p-AMPK) was increased in the proximal intestinal mucosa of $NT^{-/-}$ mice fed standard diet compared with wild type (Extended Data Fig. 5a). p-AMPK expression was decreased in the proximal intestine of $NT^{+/+}$ mice after olive oil gavage but restored to control levels with SR 48692 pretreatment (Extended Data Fig. 5b). Treatment of FHs 74 Int and RIE-1 cells with oleate led to an increase in p-AMPK (Extended Data Fig. 5c), which was reduced by NT pretreatment (Fig. 2g; Extended Data Fig. 5d). Pharmacological activation of AMPK with AICAR (5-aminoimidazole-4-carboxamide-1-β-D-ribofuranoside) further increased oleate-stimulated p-AMPK (Fig. 2h) and concomitantly decreased FA absorption (Fig. 2i); these effects were blocked by NT pretreatment. NT-mediated suppression of p-AMPK was prevented by either NTR1 or NTR3 knockdown (Extended Data Fig. 5e, f). Knockdown of the upstream AMPK kinase Ca^{2+}-calmodulin-dependent protein kinase kinase (CaMKK2)[19,20], but not liver kinase B1 (LKB1)[21], decreased oleate-stimulated p-AMPK (Extended Data Fig. 5g). Moreover, overexpression of CaMKK2 attenuated NT-mediated suppression of p-AMPK (Extended Data Fig. 5h). Together, these findings suggest that NT, acting through NTR1 and/or NTR3, increases FA absorption through suppression of CaMKK2-mediated AMPK phosphorylation.

Drosophila provide a powerful model system to better understand molecular mechanisms regulating human metabolic disorders. To further establish the role of NT on intestinal lipid absorption and AMPK regulation, human full-length NT cDNA was expressed in *Drosophila* midgut EE cells using the EE cell-specific driver *Gr36C*-Gal4 [22] (see colocalization with EE-specific transcription factor Prospero [23,24]; Extended Data Fig. 6a, b); mature $NT^{1–13}$ peptide was detected in larval gut (3.1fg/gut) and *Drosophila* S2 cells transfected with NT cDNA (Extended Data Fig. 7). Compared to control, NT expression markedly increased lipid droplets in midgut of 7d adult (Fig. 3a) and larvae (Extended Data Fig. 6c) fed a standard diet, and also increased the accumulation of lipid droplets in oenocytes (Fig. 3b)

and fat bodies (Fig. 3c) of *Gr36C*-NT 3rd instar larvae. Next, we used a diet-induced obesity model in *Drosophila*[25] to demonstrate increased lipid droplets in the midgut of control flies fed HFD compared with flies fed a standard diet. NT expression dramatically increased lipid accumulation in the midgut (Fig. 3d) and total body TG levels (Fig. 3e) with either a standard diet or HFD, suggesting that NT promotes efficient lipid absorption, and that this effect is further enhanced by increased fat concentration. Consistently, we also found that NT expression decreased gut p-AMPK levels in both adults and larvae (Fig. 3f; Extended Data Fig. 6d). These findings suggest that, similar to mice, the effects of NT on lipid absorption are mediated, in part, through AMPK regulation. Indeed, we found that AMPK overexpression decreased, whereas AMPK knockdown increased lipid droplets in the midgut of 7d adults (Fig. 3g) and the midgut, fat body and oenocytes of larvae (Extended Data Fig. 6e–g).

To identify the endogenous *Drosophila* NTR, we carried out a targeted RNAi screen in S2 cells; expression of NT or treatment with NT peptide consistently decreased p-AMPK (Extended Data Fig. 8a, b). Among the three potential *Drosophila* NTRs[26,27], RNAi of CG9918 (Pyrokinin 1 receptor, PK1-R), but not CG8784 or CG8795, blocked the decrease in p-AMPK levels in NT-expressing cells (Extended Data Fig. 8a). NT's effect does not appear to be due to interference with PK-1 signaling, since PK-1 (encoded by *Capability*) knockdown did not alter p-AMPK levels (Extended Data Fig. 8d). Knockdown of CG9918 expression in ECs using *Myo1A*-Gal4 to drive UAS-CG9918 RNAi (TRiP 27539) expression in flies also expressing NT driven by the EE cell-specific tachykinin (TK) promoter[28,29] markedly attenuated NT-induced lipid droplet accumulation (Extended Data Fig. 8c). These results indicate that NT increases lipid accumulation, at least in part, through CG9918, an NTR-like receptor that shares 32% identity and 50% similarity with mouse NTR1 (Extended Data Fig. 8e), suggesting an evolutionarily conserved function for NTR signaling in lipid uptake.

The mouse and *Drosophila* data prompted us to assess the possible role of NT in the development of obesity and its metabolic complications in humans. Fasting plasma concentrations of pro-NT were analyzed from 4,632 middle-aged subjects of the population-based Malmö Diet and Cancer Study Cardiovascular Cohort[9] (Extended Data Table 1). The age- and sex-adjusted likelihood of being obese, abdominally obese and insulin resistant significantly increased across quartiles of pro-NT plasma levels ($p = 0.01$, 0.001 and <0.0001, respectively, Table 1). Continuous values of pro-NT were also significantly related to continuous values of body-mass-index (BMI), waist circumference and homeostasis model assessment of insulin resistance (Extended Data Table 2). Among non-obese subjects, the risk of developing obesity during an average follow-up time of 16.5 ± 1.5 years increased gradually with pro-NT quartiles, independently of baseline BMI, age and gender ($p < 0.0001$, Table 1). Importantly, non-obese subjects in the top quartile of baseline pro-NT levels had greater than double the risk of developing obesity compared to those in the lowest quartile (odds ratio = 2.05, 95% CI: 1.38 – 3.06). Whereas the cross sectional relationship between pro-NT and obesity became non-significant after additional adjustment for insulin resistance, the prospective relationship between pro-NT and risk of new-onset obesity remained highly significant ($p=0.001$) after adjustment for insulin resistance (data not shown). Thus, pro-NT levels strongly predict new onset obesity in a graded manner, which is

independent of baseline BMI and insulin resistance. These findings in adults warrant further prospective studies to evaluate whether pro-NT levels can be used to predict future obesity in children and adolescents.

Our findings demonstrate a critical role of NT in high fat diet-induced obesity that involves decreased AMPK activation and increased intestinal lipid absorption. Moreover, we identify increased pro-NT levels as a strong risk factor of human obesity. From an evolutionary perspective, metabolically “thrifty” genes, like NT, are highly beneficial to ensure the efficient absorption of all ingested fats, but with the abundance of fats in typical Western diets, NT can have a detrimental effect by contributing to increased fat storage, obesity and related metabolic disorders.

Methods

Reagents

Phospho-AMPKα (Thr172) (2535), AMPKα (2532), LKB1 (3050), phospho-Akt (Ser-473) (4058) and pan-Akt (4691) antibodies were from Cell Signaling Technology (Danvers, MA). NTR1 antibody (sc-374492) was from Santa Cruz Biotechnology (Dallas, TX). CaMKK2 (ab168818), NTR3 (ab16640), and F4/80 (ab100790) antibodies were from Abcam (Cambridge, MA). FLAG (F1804) and β-actin (A5316) antibodies were from Sigma-Aldrich (St. Louis, MO). AICAR was from Cayman (Ann Arbor, MI). Oleate sodium, $NT_{1–13}$, glucose and human insulin were from Sigma. Deuterated oleic acid (CLM-460-PK) was obtained from Cambridge Isotope Laboratories (Tewksbury, MA). SR 48692 was from Tocris (Minneapolis, MN). Lipofectamine® RNAiMAX and LTX Reagent with PLUS™ transfection reagents and Trizol were from Life Technologies (Grand Island, NY). pSG5-FLAG-CaMKK2 rat FL was a gift from Anthony Means[30] (Addgene plasmid #32449, Cambridge, MA). Primers for RT-PCR were from Integrated DNA Technologies (Coralville, IA).

siRNA and sequences

ON-TARGETplus SMARTpool and ON-TARGETplus Non-targeting Control Pool siRNAs were purchased from GE Dharmacon (Lafayette, CO). The sequences are as below.

Human LKB1: i) UGACUGUGGUGCCGUACUU, ii) GCUCUUACGGCAAGGUGAA, iii) UGAAAGGGAUGCUUGAGUA, and iv) GAAGAAGGAAAUUCAACUA.

Human CaMKK2: i) GUGAAGACCAUGAUACGUA, ii) GGAUCGUGGUGCCGGAAAU, iii) GAUCAAAGGCAUCGAGUAC, and iv) ACAGUAAGAUCAAGAGUCA.

Human NTR1: i) GGACUCCGUUCCUCUAUGA, ii) GCAACACGGUGACGGCGUU, iii) GAGCACAGCACAUUCAGCA, and iv) GAACACCGACAUCUACUCC.

Human NTR3/SORT1: i) GAGACUAUGUUGUGACCAA, ii) GAGCUAGGUCCAUGAAUAU, iii) GAAGGACUAUACCAUAUGG, and iv) GAAUUUGGCAUGGCUAUUG.

Rat NTR1: i) GGGCACACACAACGGUUUA, ii) CCGAAAUGGAAGCGACGUU, iii) CUACGUUCCUCUUCGAUUU, and iv) GCUACUAUUUCCUGCGUGA.

Rat NTR3/Sort1: i) ACAAAUGGGUACCGGAAAA, ii) GAACACAGCAACCGUCCUA, iii) AAGACAUCCUUGAGCGCAA, and iv) AAGCAGAAUUCCAAGUCGA.

Mice

All procedures were approved by the Institutional Animal Care and Use Committee of the University of Kentucky. $NT^{-/-}$ mice and their wild type littermates ($NT^{+/+}$) were bred from $NT^{+/-}$ mice and randomly grouped for all experiments. Mice were maintained with a 14h light/10h dark cycle and provided with food and water *ad libitum*. For diet-induced obesity studies, male and female $NT^{+/+}$ and $NT^{-/-}$ mice were placed on a 60% HFD or 10% LFD (catalogue no. D12492 and D12450B, respectively; Research Diets, New Brunswick, NJ) at weaning for 22–24wks. Body weight (BW) and food intake were measured weekly. Food intake was measured for each cage (3–5 mice per cage) and divided by mouse number to obtain total grams consumed per mouse per week. All mice used were 4–6 months old unless otherwise indicated. For chronic SR 48692 treatment on HFD-fed mice, male C57BL/6 mice (2-mo-old) were obtained from Taconic. After one week acclimation, mice were placed in individual cages, started on HFD, and after one week were divided into 2 groups one of which received SR 48692 (dissolved in sterile diH_2O by brief sonication, 2.5 mg/kg BW [31–33] and the other vehicle twice/day (8am and 8pm) by gavage. BW and food intake were measured weekly.

Human intestinal samples

Surgical samples of duodenum and colon were obtained from de-identified donors through the Markey Cancer Center Biospecimen and Tissue Procurement Shared Resource Facility. All samples were obtained after informed consent according to a protocol approved by the Institutional Review Board of the University of Kentucky Medical Center (UKMC). Tissues were processed within 1 h after resection; the mucosal layer was sharply dissected from the underlying seromuscular layer and collected in multiple 3 to 5 mm sections for western blotting.

Cell lines, transfection and treatment

FHs 74 Int human small intestinal epithelial cells[34] were purchased from ATCC (Manassas, VA) and maintained in Hybri-Care Medium ATCC 46-X supplemented with 30 ng/ml epidermal growth factor (Sigma-Aldrich) and 10% FBS. RIE-1 rat intestinal epithelial cells[35] were maintained in *DMEM containing 2 mM L-glutamine, 4500 mg/L glucose and* 10% FBS. FHs 74 Int cells were tested for authentication via STR profiling in April 2015 by Genetica DNA Laboratories (LabCorp Specialty Testing Group; Burlington, NC) using the commercially available PowerPlex® 16HS amplification kit (Promega Corporation) and GeneMapper ID v3.2.1 software (Applied Biosystems). Authentication was confirmed by a

100% match in comparison to the reference STR profile from ATCC (FHs 74 Int; ATCC® CCL-241™). The cell lines are not listed in the ICLAC database. In addition, both cell lines were tested for mycoplasma contamination via PCR (e-Myco Plus kit; iNtRON Biotechnology) and were found to be negative. Reverse transfection was performed using RNAiMAX (for siRNA) or LTX with PLUS™ (for plasmid) transfection reagents. Final siRNA concentrations were used at 20 (NTR3), 40 (LKB1, CaMKK2) or 100 (NTR1) nM. Cells were treated after 72 h (siRNA) or 48 h (plasmid) after transfection. For combined treatment of oleate with NT, cells were pre-treated with BSA or NT (2 μM) or NT at various dosages in serum-free media as indicated in the figures for 30 min followed by oleate (0.1 mM) for 1 h or overnight. For treatment with oleate alone, cells were treated with BSA or oleate at different concentrations as indicated in the figures for 1 h in serum-free media.

Western blotting

Tissues and cells were lysed with lysis buffer (Cell Signaling Technology), and equal amounts of protein were resolved on 4–12% NuPAGE BisTris gels (Life Technologies), electrophoretically transferred to polyvinylidene difluoride (PVDF) membranes, and western blotting was performed as previously described[36,37]. p-AMPK expression was analyzed by densitometry and normalized to total AMPK expression using NIH ImageJ software from 3 separate experiments. Data are presented as fold change.

Histology and immunohistochemistry (IHC)

Tissues were fixed in 10% neutral-buffered formalin, embedded in paraffin, and sectioned (5 μm). H&E staining was performed using standard techniques. For H&E and oil red O (ORO) staining, liver tissues were collected from male $NT^{+/+}$ and $NT^{-/-}$ mice fed HFD for 24 weeks after weaning. For ORO staining, liver tissues were fixed in 10% neutral-buffered formalin, equilibrated in 30% sucrose, embedded in OCT compound and snap-frozen in liquid N_2. Frozen sections were stained with ORO (Sigma-Aldrich) for lipid deposition using standard methods. Adipocyte size was measured as described previously[38]. Briefly, sections of epididymal adipose tissue from each mouse were photographed under ×100 magnification. In a square measuring 700 × 700 μm (*x*- and *y*-axis, respectively), adipocyte size and number were measured using NIS Elements BR.3.10 software. A criterion for inclusion of measurements was a circularity of adipocytes superior to 0.33 [shape of cells; from 0 (thin shape) to 1 (perfect circle)]. IHC was performed and visualized by Dako EnVision Systems (Burlington, Ontario, Canada) following the product instruction.

Reverse transcription-polymerase chain reaction (RT-PCR)

Total RNA was isolated from cells using RNeasy Kit (Qiagen, Valencia, CA) according to the manufacturer's instructions. RT-PCR analysis of *NTR1, 2 and 3* was performed using cDNA synthesized from 1 μg of total RNA. *β-actin* was used as the internal control. The primers included: human *NTR1*: 5′-TCATCGCCTTTGTGGTCTGCT-3′ and 5′-TGGTTGCTGGACACGCTGTCG-3′; human *NTR2*: 5′-GTCTCCTCAGCTTCATCGTAT-3′ and 5′-TCCCCAAAGCCTGAAGCTGTA-3′; human *NTR3* (*SORT1*): 5′-AGAATGGTCGAGACTATGTTG-3′ and 5′-AAGAGCTATTCCAAGAGGTCC-3′; rat *Ntr1*: 5′-GAGAAGCCCCCAAAATTCTC-3′ and 5′-CAAGGACCCAGTGCAGGTAT-3′; rat *Ntr2*: 5′-ACTCGCTCATCTTCGCATTT-3′

and 5′-TGGGACCACACGAAGTTGTA-3′; rat *Ntr3* (*Sort1*): 5′-TTTCAAGCTGTGCTTTGTGG-3′ and 5′-AGTTCTCTGAACGGGAGCAA-3′. *β-actin*: 5′-TCACCAACTGGGACGACATG-3′ and 5′-ACCGGAGTCCATCACGATG-3′. The PCR products were analyzed on a 2% agarose gel.

Glucose and insulin tolerance tests

Insulin (ITT) and glucose (GTT) tolerance tests were performed on 6h-fasted male $NT^{+/+}$ and $NT^{-/-}$ mice fed HFD for 24 weeks after weaning. Glucose values were measured using One Touch Ultra from LifeScan (Wayne, PA) by tail snip. Glucose (1.5g/kg body weight) and human insulin (0.75U/kg body weight) were injected intraperitoneally (i.p.) after baseline glucose levels were established in each mouse, and blood glucose levels were measured 15, 30, 60 and 120min after injection.

Metabolic Studies

Whole body composition parameters were measured in male $NT^{+/+}$ and $NT^{-/-}$ mice fed either LFD or HFD for 24 weeks after weaning by EchoMRI-5000 Whole Body Composition (Echo Medical System, Houston, TX) using Magnetic Resonance Relaxometry to precisely measure total body fat, lean mass, body fluids and total body water in conscious mice. A TSE LabMaster indirect calorimetry system (TSE-Systems Inc., Chesterfield, MO) was used to simultaneously quantify energy expenditure, energy intake, locomotor activity, and respiratory exchange ratio (RER). Mice were acclimated to the chambers for 7d, to permit recovery from the weight loss initially experienced by obese mice. Recordings were performed for 5d, yielding three full 24h periods of data. Feeding and activity data were collected continuously; O_2 and CO_2 levels for energy expenditure and RER calculations were collected at 30min intervals. Resting energy expenditure values were calculated from data collected between 9 AM and 6 PM, filtered to remove points at which activity was greater than 150 counts for that interval.

For hepatic TG and cholesterol measurements, liver tissues were collected from male $NT^{+/+}$ and $NT^{-/-}$mice fed HFD for 24 weeks after weaning; TG and cholesterol were extracted as described previously[39] and analyzed by LC-MS coupled with electrospray ionization tandem using stable isotope dilution[40] performed on AB Sciex 4000 Q-Trap instruments. Fasting plasma glucose was analyzed using a Glucose Colorimetric Assay Kit II (BioVision) and insulin using a Mouse Insulin ELISA kit (Mercodia Inc, Winston Salem, NC). To monitor insulin secretion in response to glucose stimulation, plasma insulin and glucose levels were measured in mice (fed standard chow after weaning) that had been fasted overnight and subsequently given glucose (2 g/kg body weight) by gavage (i.e., oral glucose tolerance test). Blood was collected from tail snip before (0min) or 15, 30, 60 and 120min after gavage. Insulin and glucose levels were measured using Glucose Colorimetric Assay Kit II and Mouse Insulin ELISA kit as described above. Plasma insulin levels were also determined in mice that were either fasted for 16 h or fasted for 16h with refeeding for 4 h; blood was collected from inferior vena cava (IVC). For fecal TG assay, mice were housed in individual cages for 4 d, day 4 fecal samples were dried and ground, lipid was extracted from 50 mg feces, and TG was measured by LC-MS.

Body length measurements

Anal-nasal length was measured following isoflurane anesthesia of male and female $NT^{+/+}$ and $NT^{-/-}$ mice (7-mo-old).

Fecal weight measurements

Male $NT^{+/+}$ and $NT^{-/-}$ mice fed either normal chow (NC) or HFD for 24wks after weaning were separated into individual cages and fecal pellets were collected and weighed daily for 4 d. Fecal weights from day 4 were averaged for wild type and NT deficient mice.

Small intestinal characterization

The entire small intestine (SI), from the gastric pylorus to the ileocecal valve was dissected from anesthetized male $NT^{-/-}$ and $NT^{+/+}$ mice (7-mo-old). The SI length was measured and then opened longitudinally, washed in cold saline to clear the luminal contents, dried briefly on a paper towel and weighed. The SI was divided 5cm distal from the pyloric junction and the jejunoileum was divided into equal proximal and distal fragments. Proximal fragments were fixed in 10% neutral-buffered formalin for 24h, and "Swiss rolls" [41] were sectioned (5 μm) for H&E staining. H&E stained sections were imaged on an Aperio ScanScope XT™ slide scanner at 20x. Villus height and crypt counts were determined using Aperio ImageScope v11.2.0.780 software. Crypts in a 1mm field were counted; 10 fields were analyzed per section. Villus height was measured from 10 well-oriented villi on each slide.

Lipid absorption studies

For olive oil administration and ORO analysis, male $NT^{+/+}$ and $NT^{-/-}$ mice on NC were fasted overnight, fed olive oil (17 μl/g BW) by gavage, and sacrificed either before (control), or 30 min and 60 min after gavage. The intestine was resected from the ligament of Treitz to the ileocecal junction, divided into proximal, middle, and distal segments of equal length, washed with cold saline, and the proximal segment was processed for frozen sectioning and ORO staining using standard protocols.

For $^{13}C_{18}$-OA experiments, male $NT^{+/+}$ and $NT^{-/-}$ mice on NC were fasted overnight, fed $^{13}C_{18}$-OA (480 μg/g body weight) mixed in olive oil (10 μl/g body weight) by gavage, sacrificed either 0 or 30min later, and proximal intestinal segments were collected as described above. To detect plasma level of $^{13}C_{18}$-OA, mice were given $^{13}C_{18}$-OA as above and blood was collected from tail snip either before (0h), or 1, 2 and 3h after gavage. Lipid was extracted from proximal intestines and plasma[42] and $^{13}C_{18}$-OA levels were determined by direct infusion nanospray FT-MS (Orbitrap Fusion™ Tribrid™ Mass Spectrometer, Thermo Scientific, Waltham, MA) using a modification of a previous method[43]. Briefly, aliquots of the lipid extracts were diluted twenty-fold in isopropanol:chloroform:methanol (4:2:1), introduced into the TriVersa NanoMate® (Advion, Inc., Ithaca, NY) and analyzed on the Orbitrap Fusion in negative ion mode to estimate the appropriate amount of d34-OA to spike. Lipid extracts were then spiked with a known concentration of d_{34}-OA and re-analyzed. The nanospray conditions on the Nanomate were as follows: 15 μl of sample injection, 16min of delivery time, 0.4 psi of gas pressure, and 1.5 kV of negative applied voltage. The Orbitrap Fusion MS analysis conditions were as follows: mass resolution of 450,000 with lock mass using internal calibrant, scan range of m/z 150 – 1600, % S-Lens RF

Level of 60, $1.0e^5$ for AGC Target, 100 msec maximum injection time, and 10 averaged microscans. The ion transfer tube temperature was 275°C, and the experimental mass accuracy was ± ~1 ppm. The unlabeled, ^{13}C-labeled, and d_{34}-OA were assigned based on their respective accurate mass of 281.24860, 299.30899, and 314.45574; unlabeled and ^{13}C-labeled OA were then quantified against the internal d_{34}-OA standard using their respective peak intensity.

For NT "rescue" experiments, male $NT^{+/+}$ and $NT^{-/-}$ mice on NC were fasted overnight, fed saline or olive oil (17μl/g body weight) by gavage, injected i.p. with saline or NT (3600 nmol/kg body weight), and, following sacrifice 60 min later, proximal intestinal fragments were dissected as described above and further divided into proximal and distal halves that were either processed for ORO staining or used for TG quantification, respectively, as described previously with modifications[44]. Briefly, intestinal tissues were homogenized in 200 μl of 0.5% Tween-20 in PBS, heated for 5 min at 70°C, homogenates were microcentrifuged (3 min), and TG measurements were performed on the supernatants using a Triglyceride Determination Kit (Sigma-Aldrich) [44] according to the manufacturer's instructions.

For *in vitro* FA absorption or lipid accumulation studies, FHs 74 Int and RIE-1 cells (in serum-free medium) were incubated with either bovine serum albumin (BSA, fatty acid free) (Sigma-Aldrich) or BSA-conjugated BODIPY® FL C_{16} (4,4-Difluoro-5,7-Dimethyl-4-Bora-3a,4a-Diaza-*s*-Indacene-3-Hexadecanoic Acid) (Life Technologies) (5 μM) for 15min and images were obtained using an FV1000 Olympus confocal microscope (Olympus, Tokyo, Japan) using a 60x, 1.35-numerical aperture (NA) oil objective, zoom 3 and analyzed with Olympus FV10-ASW Ver.3.1b software. Florescence intensity was determined on a total of 30 cells from 3 fields (10 cells/field). Lipid accumulation, RIE-1 cells were pre-treated with or without NT for 30min followed by combination treatment of BSA or oleate (0.1 mM) with or without NT overnight. Cells were homogenized and TG measured using Triglyceride Determination Kit as described above. Experiments were repeated at least 3 times.

For acute SR 48692 treatment, one experiment was performed on male wild type C57BL/6 mice obtained from Taconic (Hudson, NY). Mice were acclimated for one week, randomly divided into control, olive oil, and olive oil + SR 48692 groups and fasted overnight. SR 48692 was dissolved in DMSO (50 mg/ml) and diluted 1:100 in saline just prior to use. Mice were injected i.p. with SR 48692 (2.5 mg/kg) [31,33] or vehicle 30 min prior to oral gavage of olive oil (10 μl/g), sacrificed after an additional 30 min, and the proximal intestine (see above) was used to determine TG content and for preparation of lysates for western blotting. This experiment was repeated in male $NT^{+/+}$ and $NT^{-/-}$ mice (7-mo-old), and proximal intestinal TG was measured as described above.

Drosophila studies

Full-length human NT cDNA was inserted into an attB-UAST backbone[45] and transgenic lines were generated using an attP2 locus and PhiC31 integration system. *UAS*-AMPK and *UAS-AMPKRNAi* (v106200) lines have been described[46,47]. *UAS-AMPKRNAi* line (TRiP #25931, Bloomington Stock Center) produced similar phenotypes to UAS-AMPKRNAi

(v106200) and was used for most experiments. The *UAS-CG9918RNAi* line (TRiP #27539, Bloomington Stock Center) has been described[48]. *Gr36C*-Gal4, *Myo1A*^{ts}-Gal4, *voila*-Gal4, and *S106*-Gal4 have been described[49–51] (FlyBase). *Myo1A*-Gal4 is specifically expressed in enterocytes[52]. In order to constitutively express NT in gut EE cells, a gut EE cell-specific TK promoter (2.0kb)[28,29] was cloned into attB-UAST lacking Gal4 binding sites followed by insertion of full-length NT cDNA and the resulting plasmid (TK-NT) was used to generate a transgenic line by insertion at the VK5 attP locus. To express NT in EE cells and knock down CG9918 by RNAi in EC cells, the following genotype was used: *yw; Myo1A-Gal4/CG9918RNAi*^{27539}; *TK-NT/+. tub-Gal80*^{ts} was used in combination with the *Myo1A*-Gal4 (resulting in *Myo*^{ts}) to suppress *Myo1A-Gal4* driven expression[52], until shifting larvae to 29°C (nonpermissive temperature) 96h after egg laying (AEL) or adult emerging. AMPK or AMPKRNAi were expressed in the fat body using the RU486-inducible GeneSwitch *S106*-Gal4 line. *S106*-AMPK or *S106*-AMPKRNAi larvae (3rd instar) were grown on RU486- (200 μM, Mifepristone, Sigma-Aldrich) or vehicle-containing food and lipid droplet accumulation in fat body and oenocytes was examined by Bodipy (Invitrogen) and immunohistochemical (α-HNF4 oenocyte marker[53]) staining. Midguts (3rd instar larvae, adult) were dissected, fixed in 4% formaldehyde in PBS for 20min, permeabilized in 0.1% Triton X-100 in PBS, and processed for either immunohistochemistry using mouse α-Pros (DSHB, MR1A) and rabbit α-NT (Abcam, ab43833) primary antibodies or lipid staining using Bodipy, Nile Red, or Oil Red O (larvae).

AMPK and p-AMPK were detected by western blot analysis using protein extracts from gastrointestinal tract (15/sample) using α-p-AMPK (Cell Signaling, #2535), α-AMPK (Abcam, ab80039) and α-β-tubulin control (DSHB, E7) primary antibodies and ECL as described.

Adult flies were fed HFD or standard fly food (cornmeal-yeast) as described[25]. Briefly, flies (5d after emerging) were collected and maintained on standard fly food for an additional 5d, split into two groups, and fed either standard fly food or standard fly food containing 20% (w/v) coconut oil for a further 5d, followed by dissection and lipid staining using Bodipy or Nile Red. *voila*-NT and *voila*-Gal4-w118 control flies were fed HFD or standard fly food as described above for TG measurement (25 flies/sample) as described[44]. Fluorescence signals were acquired on an Olympus confocal microscope and images processed with Olympus FV10-ASW Ver.3.1b.

Drosophila S2 cells[54] were transfected with ub-Gal4, UAST-NT, and individual dsRNAs[55] to inhibit the expression of NTR-like receptors CG9918 (nucleotides 11~570), CG8784 (nucleotides −72~478), CG8795 (nucleotides −203~343), Capa (nucleotides 1–455) or GFP control (nucleotides 6–606) using Effectene (Qiagen). Cells (6 x 10^6) were dissolved in lysis buffer (450 μL) 48h post-transfection, microcentrifuged (12000 rpm, 10min), and supernatants were analyzed by western blotting. For quantitative RT-PCR, cDNA was synthesized (SuperScript III First Strand Synthesis, Invitrogen) from 1.0 μg Trizol-extracted RNA and used for quantitative RT-PCR (95°C, 30sec followed by 40 cycles, 95°C, 5sec; 55°C, 30sec; 72°C, 15sec) using SYBR Green (Thermo-Fisher) and the ΔCt method (StepOnePlus Real-Time PCR System, Applied Biosystems). Primer pairs were as follows: CG9918, 5′-GAGTTTCAACGGCGGAGGAA-3′, 5′-AGCAGAGGAAGAAGCACACC3′;

CG8784, 5′-GGCGTGCTGGGTAATCTTAT-3′, 5′-CAAAGGTTGTACAGCTCCTG-3′; CG8795, 5′-GCTACGCCCTCATATTTATC-3′, 5′-GAGGTTATAGAGGTCCTGCG-3′; Capa, 5′-ATGAAATCTATGTTGGTC-3′, 5′-CCAACGCGCGGGAAGGC-3′; Actin, 5′-GCGTCGGTCAATTCAATCTT-3′, 5′-AAGCTGCAACCTCTTCGTCA-3′. All S2 cell experiments were independently repeated at least three times.

NT enzyme immunoassay (EIA)

Fifty μl of media from S2 cells transfected with ub-Gal4 and UAST-NT were used to measure NT levels using NT EIA Kit from Phoenix Pharmaceuticals (Burlingame, CA) as described previously[36,37].

LC-MS/MS analysis of NT

NT was analyzed by liquid chromatography tandem mass spectrometry (LC-MS/MS) using an LTQ-Orbitrap mass spectrometer (Thermo Fisher Scientific, Waltham, MA) coupled with an Eksigent Nanoflex cHiPLC™ system (Eksigent, Dublin, CA) through a nano-electrospray ionization source[56]. NT in the NT EIA kit (Phoenix Pharmaceutical) was used as standard. S2 cells were transfected with *ub*-Gal4 and UAST-NT or the UAST vector control, and conditioned medium was harvested after 48 h for analysis. GI tracts (350/genotype) were dissected from wild-type (*w1118*) or *Gr36C*-NT 3rd instar larvae, methanol extracted[57], extracts were dried, and dissolved in 20 μl 0.1% (*v*/*v*) formic acid in water for analysis. Samples were separated by reversed phase cHiPLC [ChromXP C18 column, 75 μm I.D. x 15 cm length, Eksigent cat# 804-00001; mobile phase A and B were 0.1% (*v*/*v*) formic acid in either water or acetonitrile, respectively; flow rate, 300 nl/min]. LC-MS/MS data were acquired in an automated data dependent acquisition mode consisting of an Orbitrap MS scan (300–1800 m/z, 60,000 resolutions) followed by MS/MS for fragmentation of the 7 most abundant ions with the collision induced dissociation method.

MS/MS fragments corresponding to $NT^{1–13}$ were identified by comparison with the NT standard, and quantified using the intensity of the NT^{3+} peak and NT standards (0.05, 0.1, 0.2, 0.5 fmole)[57].

Human population studies

The Malmö Diet and Cancer (MDC) study is a population-based, prospective epidemiologic cohort of 28,449 men (born 1923–1945) and women (born 1923–1950) from the city of Malmö in southern Sweden who underwent baseline examinations between 1991 and 1996[58]. From this cohort, 6,103 persons were randomly selected to participate in the MDC Cardiovascular Cohort (MDC-CC), which was designed to investigate the epidemiology of carotid artery disease, between 1991 and 1994[59]. Fasted plasma samples at the baseline examination were available for analysis of pro-neurotensin (pro-NT) and successfully measured in a total of 4,632 participants in the MDC-CC. Of those, complete data were available for BMI in 4,626, for waist circumference on 4,625, and for estimated degree of insulin resistance using the homeostasis model assessment of insulin resistance (HOMA-IR) (fasting blood glucose concentration x fasting plasma insulin concentration/22.5)[60] in 4,468 participants. BMI was defined as body weight in kilograms divided by the square of height in meters and obesity as a BMI ≥ 30 kg/m^2. Abdominal obesity was defined as a waist

circumference of ≥ 94 cm in males and ≥ 80 cm in females, according to the International Diabetes Federation definition[61]. Insulin resistance was regarded present in subjects belonging to the top 25% of HOMA-IR values in the MDC-CC. 'New-Onset Obesity' is defined as obesity development among non-obese MDC-CC participants who were re-examined and diagnosed with obesity after an average follow-up time of 16.5 ± 1.5 years. Pro-NT was measured in stored fasting plasma specimens (all samples were assayed in 2010) that were immediately frozen to −80° C at the MDC-CC baseline examination using a chemiluminometric sandwich immunoassay to detect a pro-NT precursor fragment (pro-NT 1–117) as described previously[62]. Analyses of blood glucose and plasma insulin were carried out at the time of baseline examination at the Department of Clinical Chemistry, Malmö University Hospital, which is attached to a national standardization and quality control system[63]. Of the 4,626 subjects with baseline data on BMI and pro-NT, 2,900 subjects were re-examined with a new measurement of BMI after a mean follow-up of 16.5 ± 1.5 years. In analyses of incident obesity, we excluded 306 subjects who were obese already at the baseline examination, leaving a total of 2,594 non-obese subjects for analysis of pro-NT in relation to incident obesity. All participants gave written informed consent, and the study was approved by the Ethical Committee at Lund University, Lund, Sweden.

Statistical analysis

Descriptive statistics including means and standard deviations were calculated and represented using bar or line graphs. Linear mixed models were implemented to compare body weight and food intake levels over time as well comparisons at each time point for other endpoints from *in vivo* experiments involving repeat measurements. Specifically, body weight growth curves were compared using linear mixed models with fixed effects for linear and quadratic terms for time and their interaction with genotype and random effects for the intercept and time factors. Contrast statements for the interaction terms in the model were used to assess differences in growth curves between genotypes. Likewise, linear mixed models were employed for body weight growth curve comparisons between vehicle versus SR 48692 with the same fixed and random effects terms as above along with baseline weight as a covariate. Total food consumption for 22 weeks was calculated and compared between genotypes and between vehicle versus SR 48692 treatment using two-sample t-tests. Furthermore, weekly food intake levels were analyzed using linear mixed models. However, since there is no clear trend in weekly food intake over time, an overall comparison of trend was not employed. Instead, a linear mixed model with fixed effects for genotype, time and their interaction and a random effect for the intercept term was employed in order to perform individual comparisons at each time point. A p-value adjustment due to multiple testing at each time point was performed using the Holm's step-down procedure. We used the Akaike Information Criterion (AIC) to evaluate the goodness-of-fit of the above linear mixed models. Two-sided, two-sample Student's t-test was employed for cell culture and *in vivo* studies involving two independent groups. One-way or two-way analysis of variance models with test for interaction between two factors was employed for multiple group comparisons of diet (LFD, HFD), mouse genotype, feeding and fasting groups, different time points of measurement, varying doses of NT treatment, SR48692 and AICAR treatments with Holm's p-value adjustment for multiple pairwise comparisons. Analysis of covariance (ANCOVA) was employed to compare genotype and diet with adjustment for the confounding effect of

mouse body weight for fat composition and energy metabolism endpoints (energy expenditure, locomotor activity, energy intake, respiratory ratio). Model-building was performed to assess equality of slopes using two-way interactions between each of genotype and diet with the body weight covariate as well as genotype and diet interactions.

For the animal studies, sufficient sample sizes were utilized to provide at least 80% power to detect large effect sizes (1.0 to 3.0 mean differences in SD units) based on two-sided, two-sample t-tests with 5% significance level. Some experiments including body weight and food intake were measured repeatedly thus affording larger statistical power. No replicate samples from *in vitro* studies were excluded in the analysis. All data from animal studies with measurement of study endpoints were included in the analysis. Experiments with slight differences in animal numbers per group were due to the number of animals that were successfully bred and not due to exclusion of certain animals and their data points. Mice within a cage were randomized to all groups in an experiment to ensure balance in treatment group assignments across all cages. The animals were randomly selected for group assignment without preference to size or other confounding factors. A different individual performed measurements on study endpoints to ensure blinding from group assignment. Furthermore, only animal IDs without information on group assignment were available to staff performing the endpoint evaluation. Parametric tests were utilized after evaluating distribution of data (e.g. percentiles, mean and median levels), test for normality (e.g. Kolmogorov-Smirnov test, if sufficient sample sizes) and test for homogeneity of variance assumptions across groups. Otherwise, data log transformation or nonparametric tests were utilized. Appropriateness of other statistical models including linear mixed models was evaluated for goodness-of-fit using the Akaike Information Criterion (AIC) and equality of slopes between groups was evaluated for the analysis of covariance (ANCOVA) models.

All subjects at the MDC-CC baseline examination were divided into ascending quartiles according to their value of fasting pro-NT. Body mass index (BMI), waist circumference and homeostasis model assessment of insulin resistance (HOMA-IR) were analyzed as dichotomous outcome variables as defined above. In cross-sectional analyses, we related baseline quartile of pro-NT to the dichotomous outcome of obesity, abdominal obesity, and insulin resistance using age and sex adjusted logistic regression models. In the analyses of incident obesity, we related baseline quartile of pro-NT to the dichotomous outcome of incident obesity using logistic regression adjusted for baseline age, sex, and BMI. Data are presented as odds ratios (95% confidence intervals), and subjects belonging to the lowest quartile of pro-NT were defined as the referent group (odds ratio =1). ‘p for trend’ denotes the p-value for linear trend over quartiles 1–4. For code availability, statistical analysis codes in SAS version 9.4 were used for analysis of in vivo and in vitro studies and SPSS version 22.0 for analysis of human data and can be accessed by contacting the senior author (BME).

Extended Data

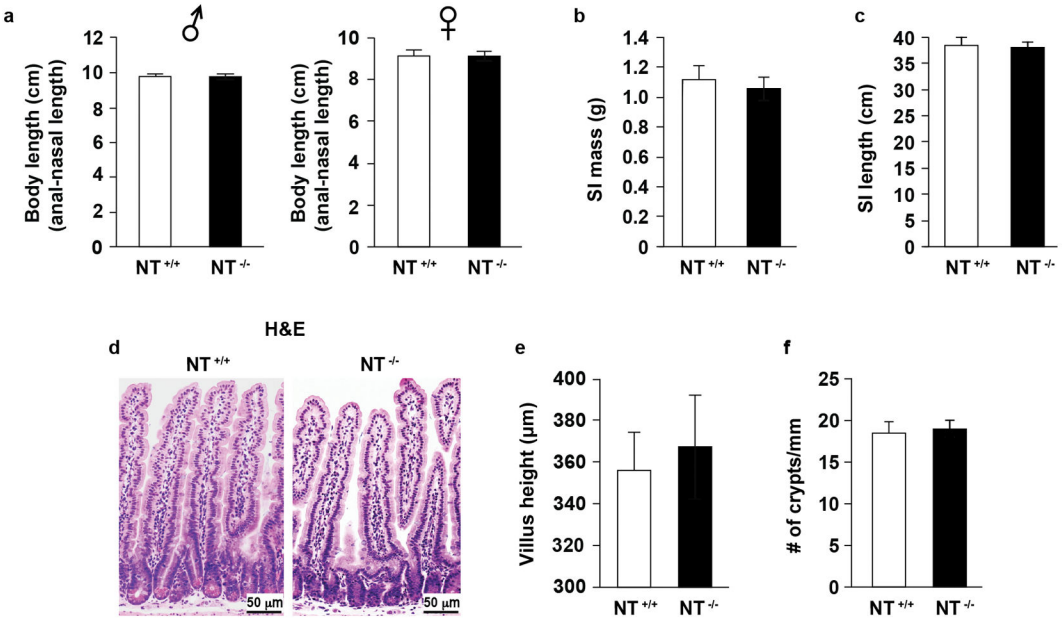

Extended Data Fig. 1. NT deficiency does not affect body length or small intestine morphology

a. Body length did not differ significantly between genotypes for either male ($NT^{+/+}$ n=13, $NT^{-/-}$ n=12) or female ($NT^{+/+}$ n=12, $NT^{-/-}$ n=12) mice. **b–f.** The average weight (b) and length (c) of the small intestine was similar between the genotypes (n=7). Proximal intestinal samples were H&E stained (d, bar=50 μm); villus height (e, n=6) and crypt numbers (f, n=6) have no significant differences between genotypes. Mice (7-mo-old) for all experiments were maintained on standard chow. All data are mean ± SD. Two-sided, Student's t-test for all figures.

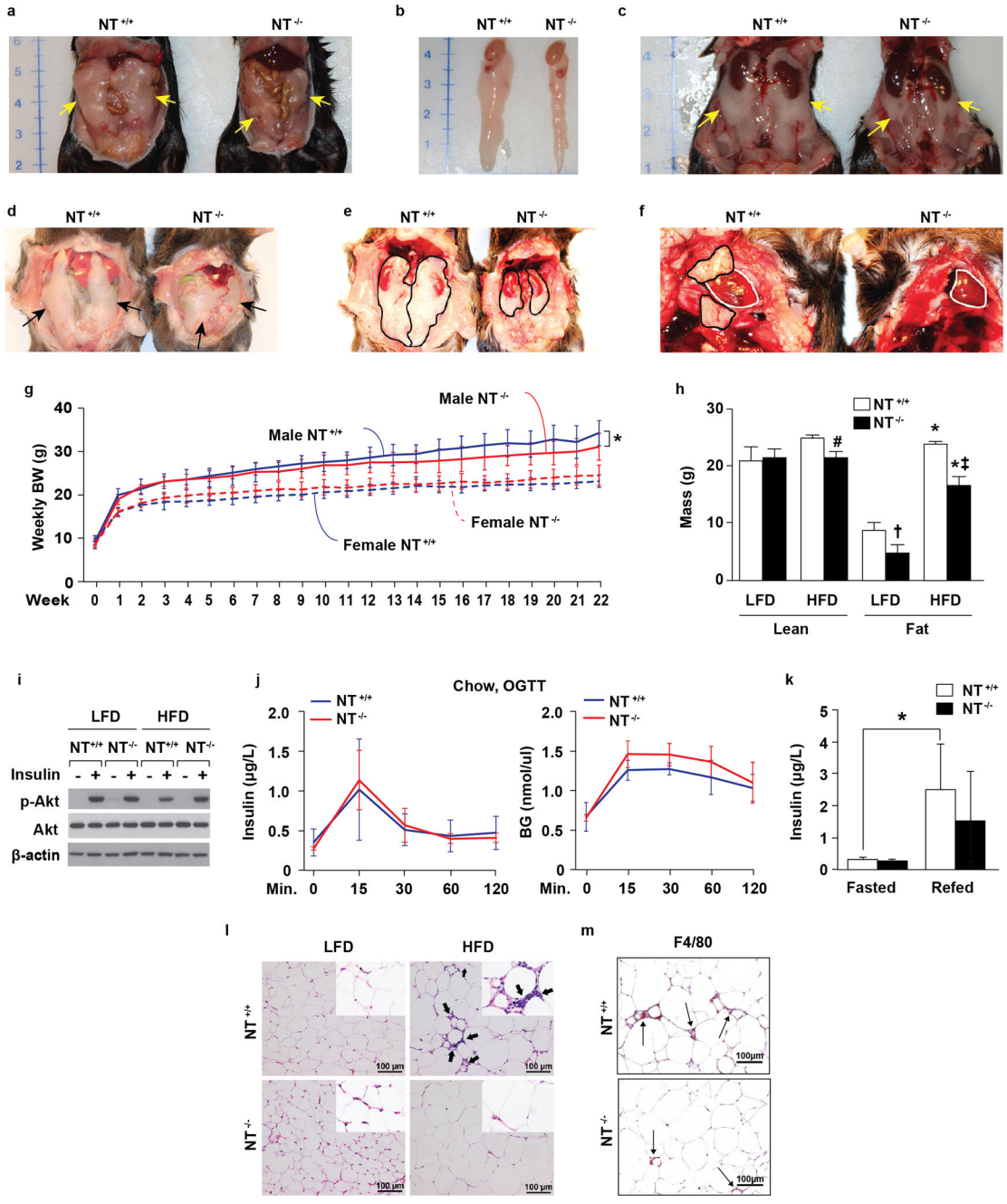

Extended Data Fig. 2. NT deficiency inhibits adiposity, inflammation and improves insulin/Akt signaling

a–c. Epididymal fat pad before (a, arrows) and after (b) dissection, and retroperitoneal fat pad (c, arrows) from male mice maintained on a normal chow (n=5). **d–f.** Representative epididymal (d, arrows), retroperitoneal (e) and pericardial fat pads (f) of male mice fed a HFD for 24wks (n=5). **g.** Weekly body weight (male $NT^{+/+}$ and $NT^{-/-}$ n=13) and (female $NT^{+/+}$ n=12, $NT^{-/-}$ n=14) of mice on a LFD for 22wks. *p<0.05 $NT^{+/+}$ vs. $NT^{-/-}$ in male mice. **h.** Fat composition in male mice fed LFD or HFD for 24wks (n=5). *p<0.05 vs. LFD fat; †p<0.05 vs. $NT^{+/+}$ LFD fat; ‡ p<0.05 vs. $NT^{+/+}$ HFD fat; #p<0.05 vs. $NT^{+/+}$ HFD lean.

i. $NT^{+/+}$ and $NT^{-/-}$ mice fed LFD or HFD for 22 wks after weaning were fasted overnight. Saline or insulin (5 units) was injected into the IVC. Five min after the injection, liver tissues were collected and protein extracts analyzed by western blot. A representative result is shown from 3 separate experiments. **j**. Male $NT^{+/+}$ and $NT^{-/-}$ mice (7-mo-old) maintained on standard chow were fasted overnight followed by glucose (2 mg/kg) administration by gavage (n=5). Blood samples were collected both prior to and at the indicated times after glucose administration for measurement of plasma insulin (*left panel*) and glucose (*right panel*) levels. No statistically significant differences in either insulin or glucose levels were apparent between genotypes. **k**. Male $NT^{+/+}$ and $NT^{-/-}$ mice (12-mo-old) fed standard diet after weaning were fasted for 16 h or fasted for 16 h and refed for 4 h (n=3). Blood was collected from IVC and plasma used to measure insulin. * $p<0.05$ vs. fasted $NT^{+/+}$ mice. **l.** H&E staining of epididymal fat pad from male mice shown in Fig. 1g demonstrating inflammatory cells (arrows) (bar=100 μm). **m.** F4/80-positive macrophages (arrows) in epididymal fat pad from HFD-fed mice (bar=100 μm) (n=5). All data are mean ± SD. Linear mixed model for g; ANCOVA with Holm's p-value adjustment for h, j, k (See Supplementary Fig. 1 for gel source data).

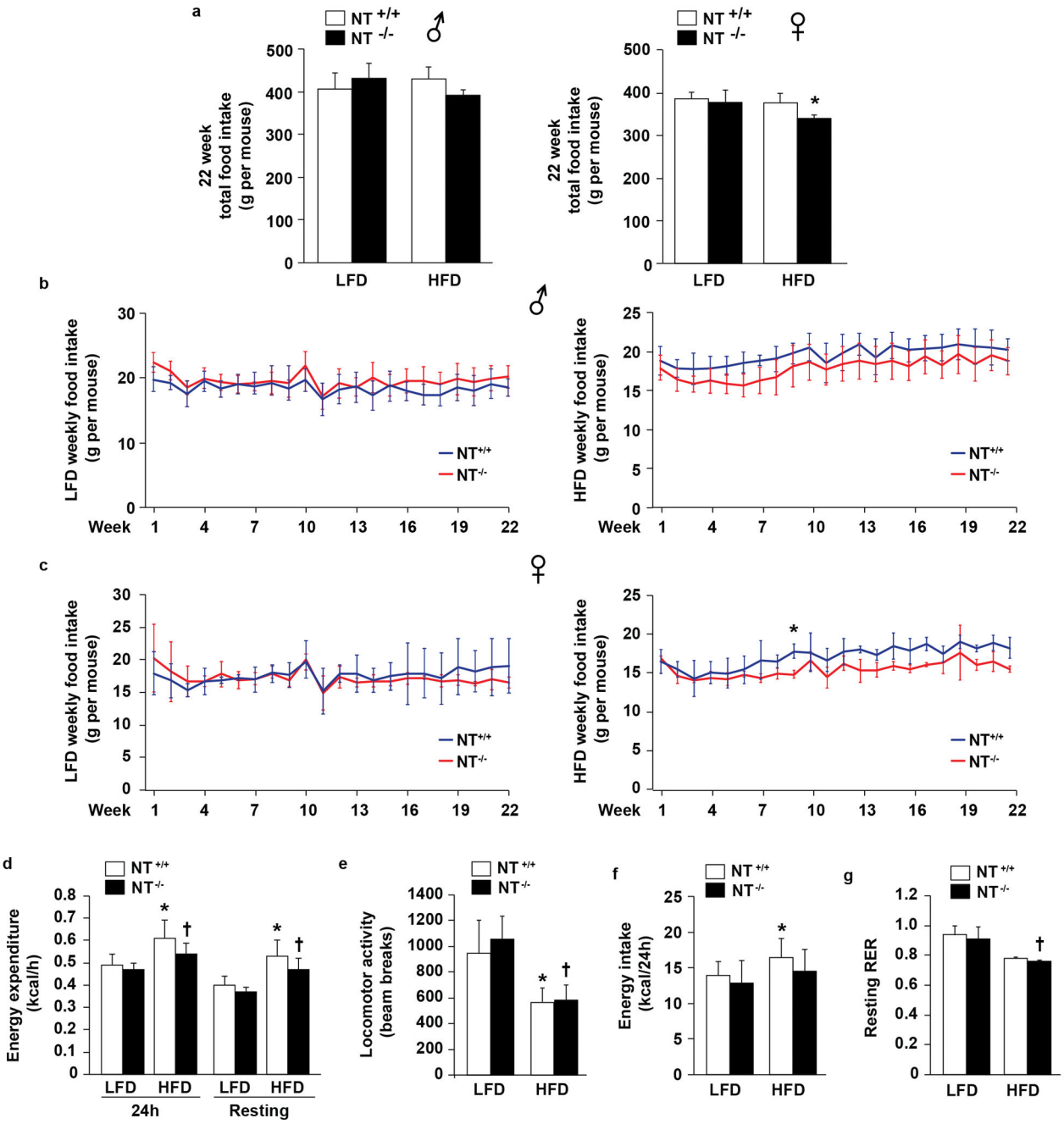

Extended Data Fig. 3. Food intake and indirect calorimetry measurements

a–c. Food intake was measured weekly for $NT^{+/+}$ and $NT^{-/-}$ male (LFD n=3 and HFD n=4) and female (LFD n=3 and HFD n=4) mice. Analysis of cumulative food intake for 22wks did not show a significant difference except in female mice fed HFD. * $p<0.05$ vs. female $NT^{+/+}$ fed HFD (a). For weekly food intake, there was no significant difference between genotypes in male mice on both diets (b) and female mice fed LFD (c, *left panel*); food intake on week 9 in female mice fed HFD reached significance between genotypes. * $p<0.05$ vs. $NT^{-/-}$ (c, *right panel*). **d–g.** Male mice on LFD and HFD diets for 24wks were placed in

individual cages and indirect calorimetric analysis performed (n=10). Energy expenditure is presented by the average kcal/h in 24h and in resting period (d). Locomotor activity represents counts of beam breaks in a 30min-period (e). Energy intake represents the food intake in kcal for 24h (f). Resting RER is presented in g. * p<0.05 vs. LFD in $NT^{+/+}$ mice; † p<0.05 vs. LFD in $NT^{-/-}$ mice. All data are mean ± SD. Two-sided, Student's t-test per diet and sex groups for a; linear mixed model for b, c; ANCOVA for d, e, f, g.

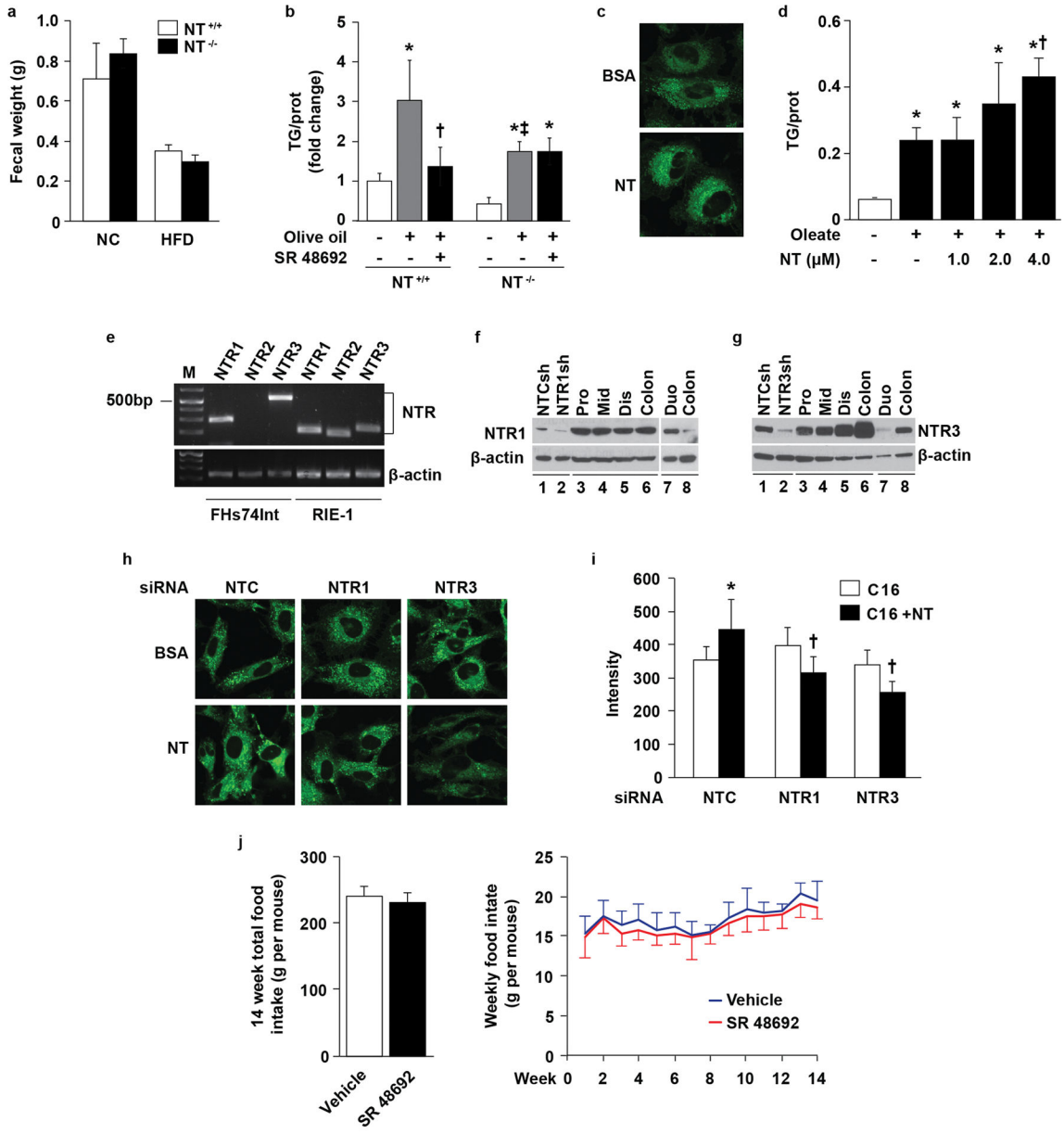

Extended Data Fig. 4. NT promotes intestinal cell lipid absorption or accumulation

a. Fecal weight of male $NT^{+/+}$ and $NT^{-/-}$ mice fed either normal chow (NC, $NT^{+/+}$ n=4, $NT^{-/-}$ n=5) or HFD ($NT^{+/+}$ n=7, $NT^{-/-}$ n=9) for 24wks; there was no significant difference between genotypes. **b.** Male $NT^{+/+}$ and $NT^{-/-}$ mice (n=4) on normal chow were fasted

overnight. Mice were injected with either saline or SR 48692 (2.5 mg/kg, i.p). Thirty min after the injection, mice were given olive oil (10 μl/g) by oral gavage and then sacrificed. The proximal small bowel was excised and intestinal TG content measured. *p<0.05 vs. saline in $NT^{+/+}$ and $NT^{-/-}$ mice; † p<0.05 vs. olive oil only in $NT^{+/+}$ mice; ‡ p<0.05 vs. olive oil only in $NT^{+/+}$ mice. **c**. RIE-1 cells were pre-treated with BSA or NT (2 μM) for 30min, followed by incubation with BSA-conjugated BODIPY® FL C_{16} for 15min, and labeled lipids were visualized by confocal microscopy. Representative images are from 3 experiments. **d.** RIE-1 cells were pre-treated with or without NT at different concentrations for 30min followed by the addition of BSA-conjugated oleate (0.1 mM) and further incubation overnight. Cells were collected, lysed and TG was measured (n=3). * p<0.05 vs. BSA only; † p<0.05 vs. oleate only. **e**. Total RNA was isolated from human (FHs 74 Int) and rat (RIE-1) small intestinal epithelial cells and RT-PCR performed using specific primers targeting human or rat NTR1, 2 and 3. **f–g**. Expression of NTR1 (f) and NTR3 (g) was analyzed by western blot from mucosa scraped from mouse proximal (pro), middle (mid), distal (dis) small bowel and colon (lanes 3–6) as well as human duodenum (duo) and colon (lanes 7–8). Proteins from HepG2 (human hepatocellular carcinoma cell line) (e, lanes 1–2) and Caco-2 (human colon cancer cell line) (f, lanes 1–2) cells stably expressing NTR1, NTR3, or control (NTC) shRNA were used as positive and negative controls. **h–i.** RIE-1 cells transfected with non-targeting control (NTC) siRNA or NTR1 or NTR3 siRNA for 72h were treated with or without NT (2 μM) for 30min followed by BSA-conjugated BODIPY® FL C_{16} (C_{16}) for 15min, and imaged by confocal microscopy to quantify fluorescence (h) and intensity (i) as described in Methods (n=30 cells). * p<0.05 vs. C_{16} in NTC siRNA; † p<0.05 vs. C_{16} plus NT in NTC siRNA. **j.** Cumulative (*left panel*) and weekly (*right panel*) food intake was measured in male wild type C57BL/6 mice fed HFD and chronically treated with either SR 48692 (n=13) or vehicle (n=12). Neither analysis demonstrated a significant difference. All data are mean ± SD. ANOVA with Holm's p-value adjustment for a, b, d, i; two-sided, Student's t-test for j (*left panel*); linear mixed model for j (*right panel*) (See Supplementary Fig. 1 for gel source data).

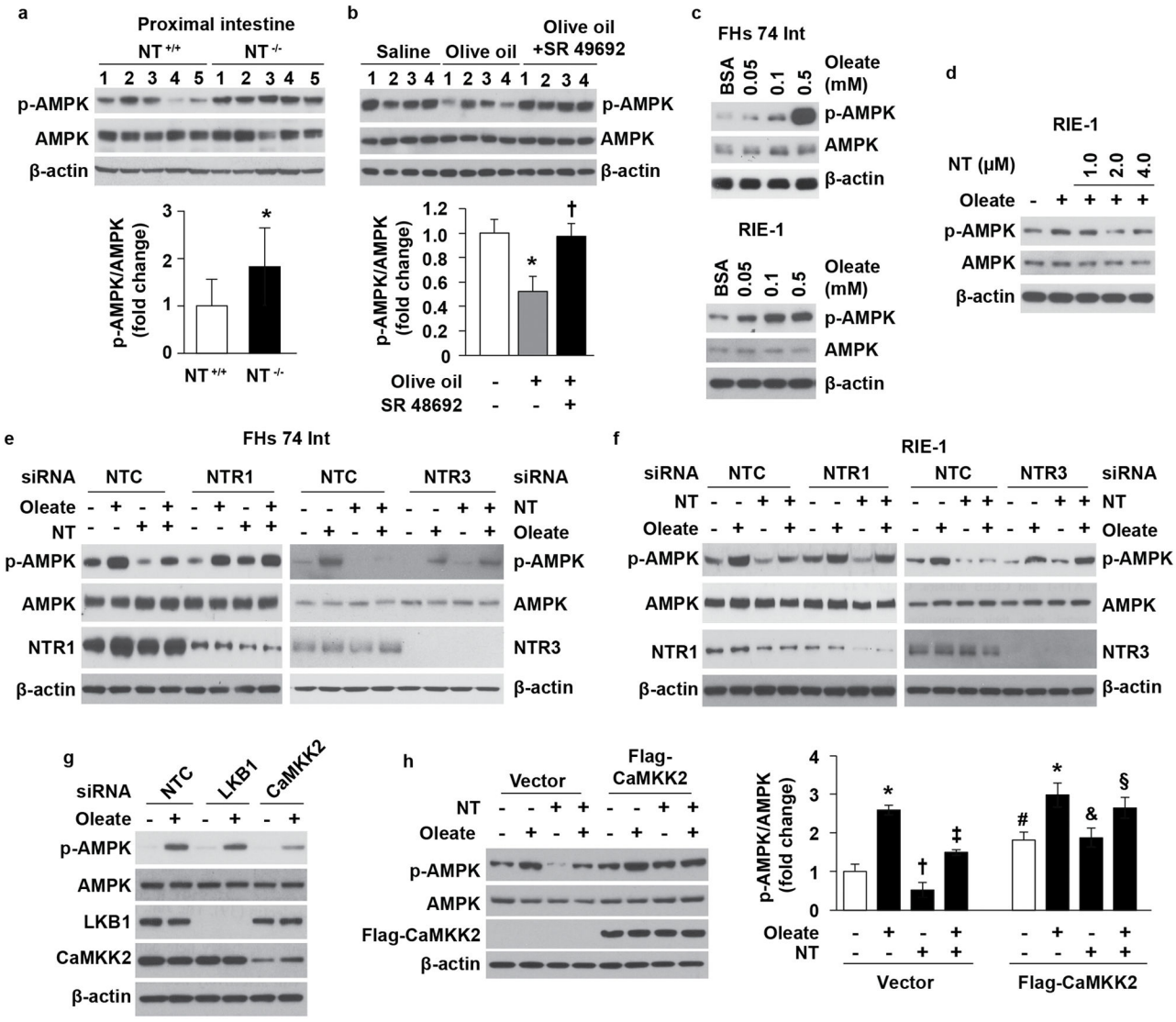

Extended Data Fig. 5. NT negatively regulates AMPK activity

a. Western blotting and densitometry of p-AMPK in proximal intestinal mucosa of male mice (12-mo-old) maintained on standard chow and fasted for 24 h (n=9). * $p<0.05$ vs. $NT^{+/+}$. **b.** Western blotting and densitometry of p-AMPK levels using samples described in (Fig. 2e, n=8). * $p<0.05$ vs. saline; † $p<0.05$ vs. olive oil alone. **c.** FHs 74 Int (*upper panel*) and RIE-1 (*lower panel*) cells were treated with the indicated concentrations of oleate for 1h and lysates were analyzed by western blotting. **d.** RIE-1 cells were pre-treated with or without NT for 30min followed by combined treatment by BSA or oleate (0.1 mM) for 1h and western blot analysis. **e.** FHs 74 Int cells transfected with either human NTR1 or NTC siRNA (100 nM)), or either human NTR3 or NTC siRNA (20 nM) as indicated for 72h were pretreated with or without NT (2 μM) for 30min followed by treatment with oleate (0.1 mM) or BSA for 1h and western blot analysis. **f.** RIE-1 cells were transfected with rat siRNAs and treated with NT and oleate as described in (e). **g.** FHs 74 Int cells transfected with LKB1, CaMKK2 or control (all 40 nM) siRNAs for 3d were pretreated with NT (2 μM) for 30min

followed by oleate (0.1 mM) for 1h and cell extracts were analyzed by western blotting. **h**. FHs 74 Int cells transfected with Flag-CaMKK2 and control vector for 48h were pretreated with or without NT (2 μM) followed by oleate (0.1 mM) for 1h and analyzed by western blotting (*left panel*); p-AMPK levels were determined as in (g) from 3 separate experiments (*right panel*). * p<0.05 vs. BSA in vector- and CaMKK2-transfected cells, respectively; † p<0.05 vs. BSA in vector-transfected cells; ‡ p<0.05 vs. oleate in vector-transfected cells; # p<0.05 vs. BSA in vector-transfected cells; & p<0.05 vs. NT alone in vector-transfected cells; § p<0.05 vs. oleate + NT in vector-transfected cells. All data are mean ± SD. Two-sided, Student's t-test for a (*lower panel*); ANOVA with Holm's p-value adjustment for b (*lower panel*), h (right panel) (See Supplementary Fig. 1 for gel source data).

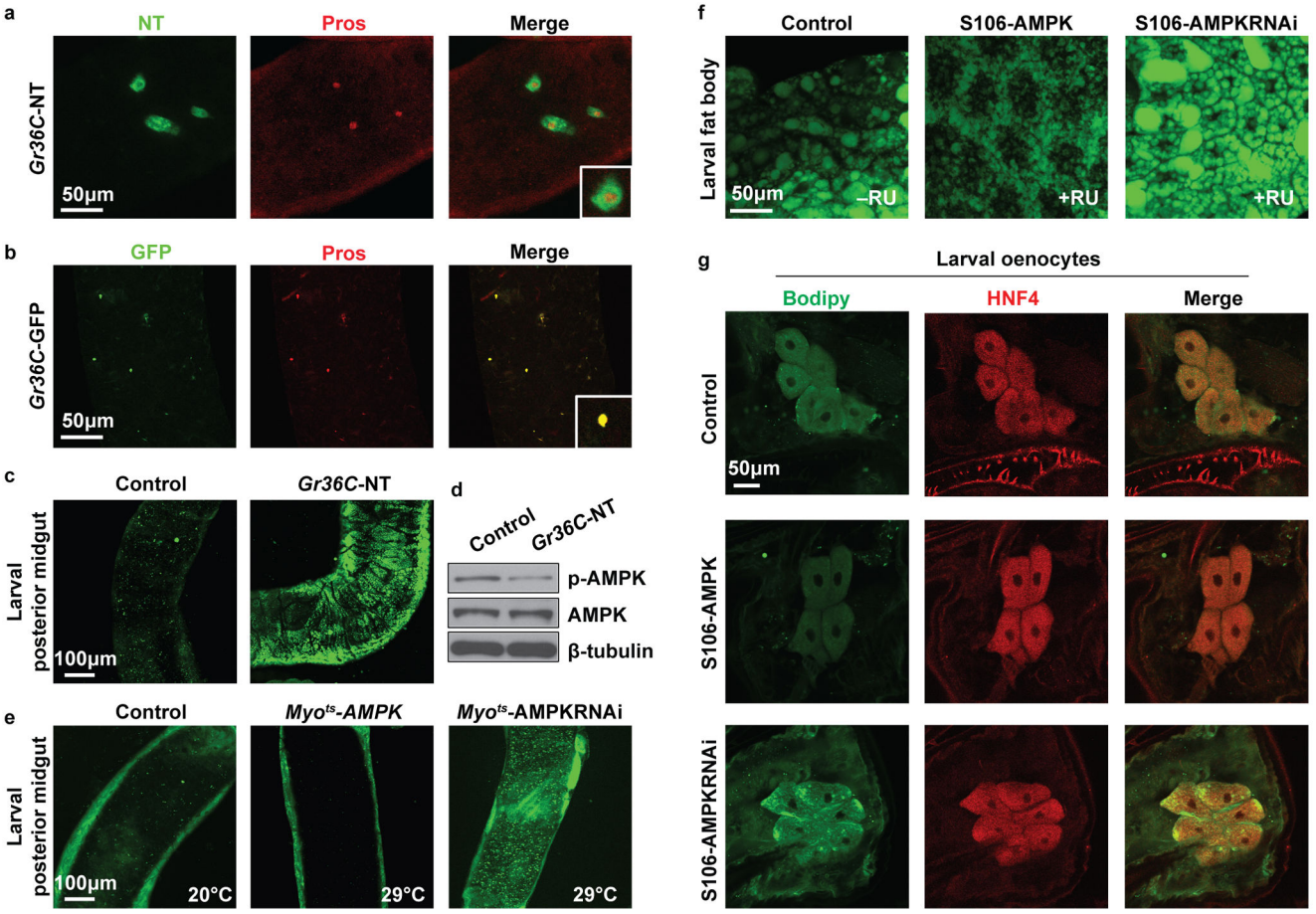

Extended Data Fig. 6. NT regulates lipid droplet accumulation and AMPK activation in *Drosophila* midgut, fat body, and oenocytes

a. Midgut from *Gr36C*-NT adult (7d) was stained for NT and Prospero (Pros). Insets in a. and b. are high magnification images of individual Pros-expressing EE cells, co-expressing either NT, or nuclear GFP (see below), respectively (n=3). Bar, 50 μm. **b.** Similar experiment using *Gr36C*-Gal4 to drive nuclear GFP expression, demonstrating co-localization of GFP and Pros in nuclei of EE cells in adult flies (7d) (n=3). Bar, 50 μm. **c.** NT expression promotes the accumulation of lipid droplets. Midguts from either control *Gr36C*-Gal4 (*left panel*, 100%, n=15) or *Gr36C*-NT (*right panel*, 100%, n=19) 3rd instar larval stained with

Bodipy. Similar results were obtained with Nile Red staining (data not shown). Bar, 100 μm. **d.** Western blot analysis of p-AMPK and AMPK levels in gastrointestinal tract of Gr36-Gal4 control and Gr36-NT 3rd instar larvae. **e.** Conditional expression of AMPK (*middle panel*, *Myo*^{ts}-AMPK, 29°C, 86%, n=14) or AMPK RNAi (*right panel*, *Myo*^{ts}-AMPKRNAi^{25931}, 29°C, 91%, n=11) leads to either suppression or enhancement of lipid accumulation (visualized with Bodipy) as compared to control (*left panel*, *Myo*^{ts}-AMPK, 20°C, 100%, n=9) 3rd instar larvae. Embryos were raised at 20°C and 96h after egg laying were switched to the nonpermissive temperature (29°C) to induce Gal4 expression. AMPK overexpression and RNAi inhibition were monitored by western blotting with AMPK antibody (data not shown). Bar, 100 μm. **f.** Similar results were obtained in 3rd instar larval fat bodies using a RU486- inducible *S106*-Gal4 driver to drive AMPK without RU486 (control, *left panel*, 100%, n=9), AMPK with RU486 (*middle panel*, 89%, n=9) or AMPK RNAi with RU486 (*right panel*, 100%, n=10) expression. Bar, 50 μm. **g.** Lipid accumulation in oenocytes (HNF-positive) visualized with Bodipy as in (e). Genotypes and fluorescent stains are indicated. Compare middle panels (100%, n=6) and bottom panels (89%, n=9) to top control panels (100%, n=8). Bar, 50 μm. (See Supplementary Fig. 1 for gel source data).

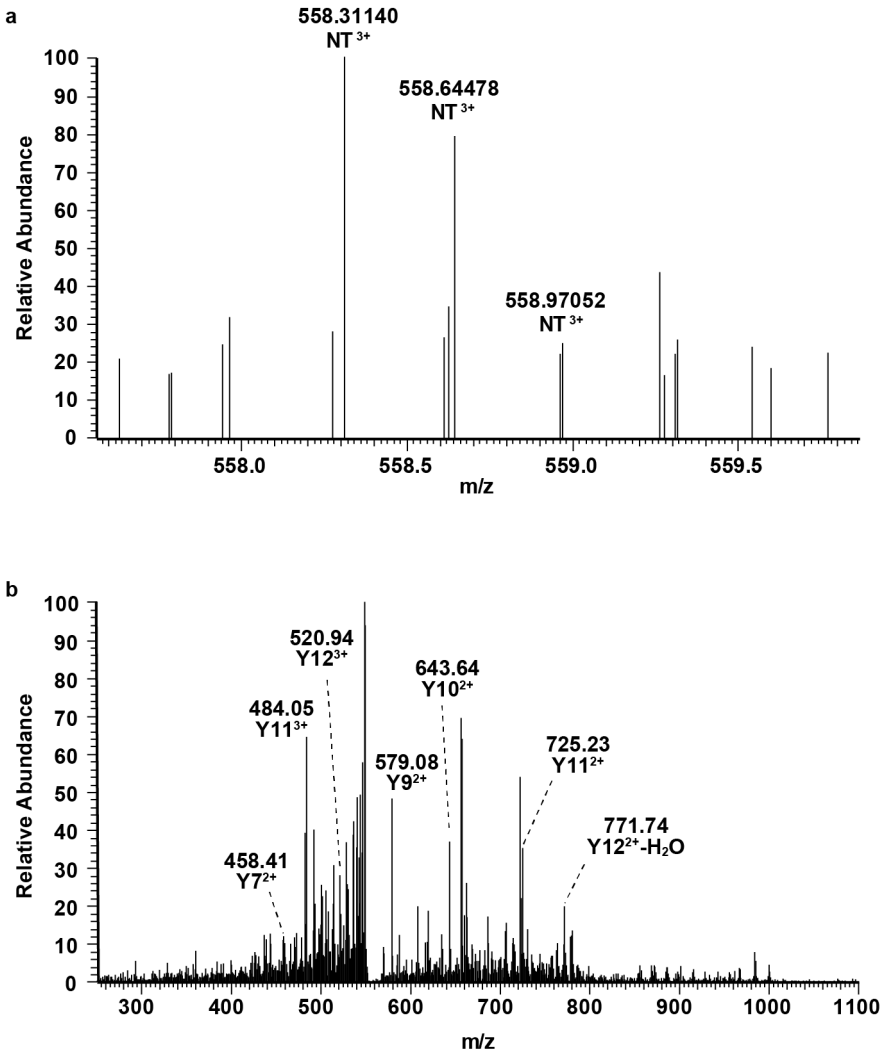

c

NT(1-13) concentration in S2 cell culture medium	67 x 10^{-12} g/ml
NT(1-13) in control fly gut	N.D.
Average amount of NT(1-13) in Gr36C-NT fly gut	3.1 x 10^{-15} g/gut

Extended Data Fig. 7. LC-MS/MS analysis of the processed NT peptide

a. The mass spectrum of the triply charged NT (NT^{3+}) peptide eluted at 18.96 min in conditioned medium of S2 cells expressing full-length human NT precursor. The labeled three peaks are the isotopic envelope of NT^{3+} with a mass accuracy less than 2 ppm from the theoretical m/z value of 585.31050. **b.** The tandem mass spectrum of the triply charged NT^{3+} peptide. The m/z values of major fragment ions are designated, confirming the peptide as biologically active 13-amino acid NT. **c.** The amount of NT in S2 medium and fly GI tracts from adult *Gr36C*-NT flies (350 guts collected for each genotype) was quantified (N.D., not detected).

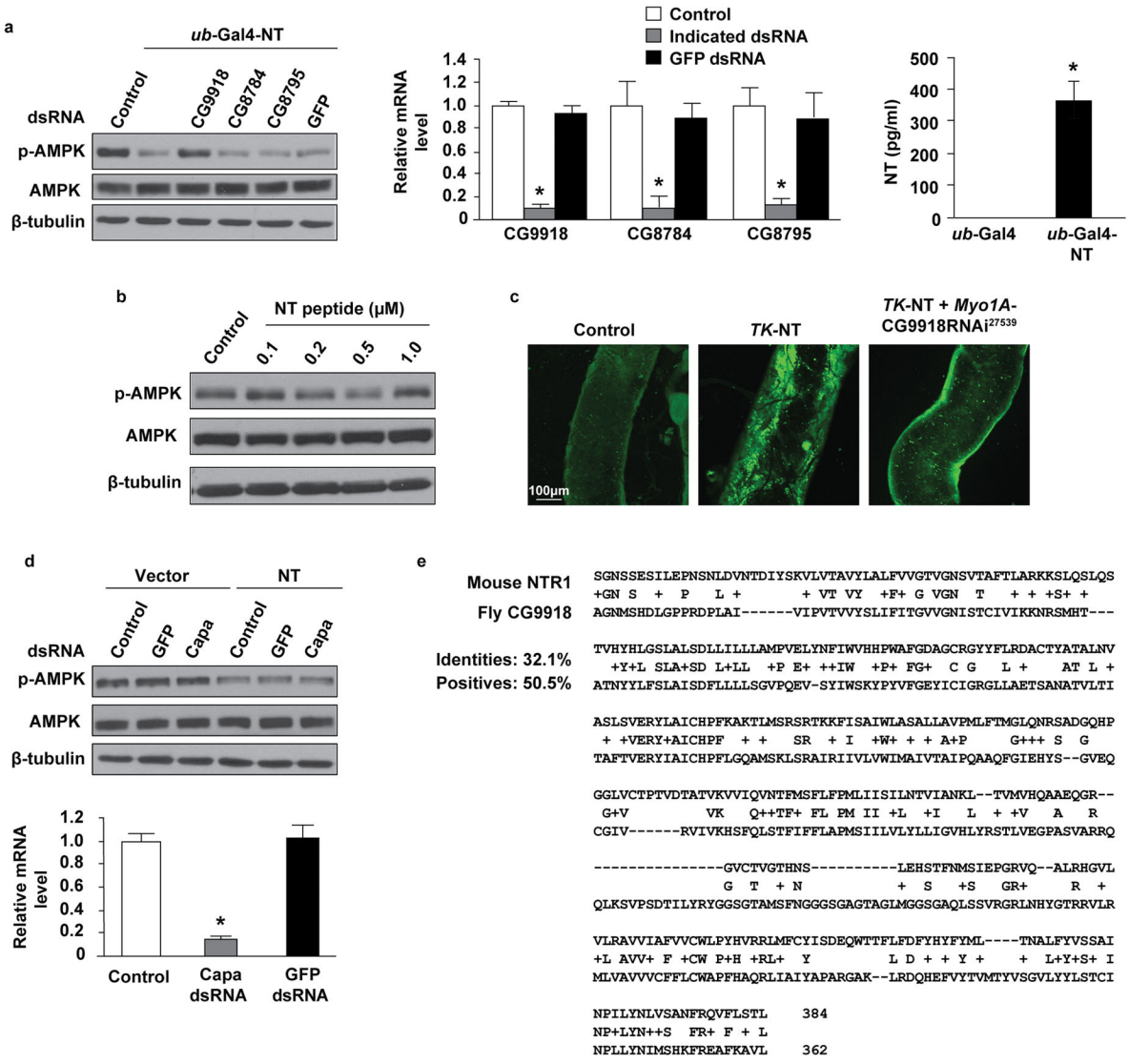

Extended Data Fig. 8. CG9918 (mouse NTR1 analog) RNAi blocks the NT-mediated decrease of p-AMPK levels in *Drosophila* S2 cells

a. S2 cells were transfected with *ub*-Gal4 plus UAST-NT (*ub*-Gal4-NT) or control (*ub*-Gal4) vector and treated with the indicated dsRNAs to knockdown individual receptors. Cell lysates were subjected to western blot with the indicated antibodies to examine the activation of AMPK (*left panel*). The efficiency of RNAi knockdown was monitored by real time-PCR (*middle panel*, n=3); * p<0.05 vs. control dsRNA. Medium from cells expressing either *ub*-Gal4 alone or *ub*-Gal4-NT was collected to examine NT levels by EIA[36,64] (*right panel*, n=6); * p<0.05 vs. *ub*-Gal4. **b.** S2 cells were treated with the indicated concentrations of NT peptide for 1h and AMPK activation was monitored as in (a). NT treatment (0.2, 0.5 μM) decreased p-AMPK to levels similar to those observed in *ub*-Gal4-NT transfected cells where NT levels reach approximately the same concentration (~350 pg/ml, 0.2 μM). **c.** Midguts of 3rd instar larvae from the indicated genotypes were stained with Bodipy to monitor the accumulation of lipid droplets. *Left panel*, *w1118* control midgut accumulates

low level of lipid (100%, n=8). *Middle panel*, larval midgut constitutively expressing NT by the TK promoter (TK-NT) accumulates high levels of lipid (100%, n=8). *Right panel*, larval midgut co-expressing TK-NT and *Myo1A*-CG9918RNAi^{27539} accumulated much lower levels of lipid (87%, n=15) compared to TK-NT midgut (*middle panel*). Bar, 100 μm. **d.** S2 cells were transfected with *ub*-Gal4-NT or control vector, treated with the indicated dsRNAs, and cell lysates were analyzed as in (a). Inactivation of Capability (Capa, CG15520), the Pyrokinin-1 in *Drosophila*, does not alter the levels of p-AMPK in either the presence or absence of NT (*upper panel*), indicating that NT prevents AMPK activation independently of Pyrokinin-1. Capa RNAi efficiency was monitored by real time-PCR (*lower panel*, n=3). * $p<0.05$ vs. control dsRNA. **e.** Amino acid sequence alignment of mouse NTR1 and *Drosophila* CG9918, identities and conserved residues (+) are indicated. All data are mean ± SD. ANOVA for a (*middle panel*), d (*lower panel*); two-sided, Wilcoxon rank-sum test for a (*right panel*). (See Supplementary Fig. 1 for gel source data).

Extended Data Table 1

Clinical characteristics of the Malmö Diet and Cancer Cardiovascular Cohort (MDC-CC).Data are given as mean ± standard deviation for normally distributed variables, and as median and interquartile range for fasting insulin concentration. Categorical data are presented as numbers (percentages). “N” denotes the number with complete data, thus, included in analyses. HOMA-IR, Homeostasis Model Assessment of Insulin Resistance (fasting plasma insulin concentration x fasting blood glucose concentration/22.5).

Characteristic	Value	N
Age (years)	57.7 ± 6.0	4,626
Female sex, n (%)	2661 (57.5)	4,626
Body Mass Index (kg/m^2)	25.8 ± 3.9	4,626
Waist circumference (cm)	84.0 ± 12.9	4,625
Fasting blood glucose (mM)	5.2 ± 1.4	4,468
Fasting insulin concentration (mU/L)	7.0 (4.0–9.0)	4,468
HOMA-IR	1.5 (0.9–2.2)	4,468

Extended Data Table 2

Association between continuous values of log-transformed fasting plasma concentration of pro-neurotensin (pro-NT) (expressed as per 1 SD increment of log-transformed value) in relation to continuous outcome values of body mass index, waist circumference and HOMA-IR in human subjects (Malmö Diet and Cancer Cardiovascular Cohort, MDC-CC).HOMA-IR = Homeostasis Model Assessment of Insulin Resistance; SD = standard deviation; SE = standard error; pro-NT = pro-neurotensin. Based on linear regression model.

Metabolic trait	β-coefficient ± SE (per SD increment of log-transformed pro-NT)	p-value
Body Mass Index (kg/m^2)	0.14 ± 0.06	0.016
Waist circumference (cm)	0.33 ± 0.15	0.026
HOMA-IR (mmol/L*mU/L)	0.13 ± 0.015	<0.001

Supplementary Material

Refer to Web version on PubMed Central for supplementary material.

Acknowledgments

We thank Donna A. Gilbreath, Catherine E. Anthony, Heather N. Russell-Simmons and Jennifer F. Rogers for manuscript preparation; Dana Napier for tissue sectioning and staining; Garretson Epperly for intestinal crypt measurements and the use of the Aperio ScanScope; Dr. Eun Y. Lee for consultation and assessment of histologic sections and immunohistochemistry; Drs. Robert Carraway, Jayakrishna Ambati, Patricia Forgez and Kathy Grzech for their suggestions and review of the manuscript; Drs. Jae Young Kwon for the *Gr36C*-Gal4 line, Marcos Vidal for the *voila*-Gal4 line, Norbert Perrimon and Tony Ip for the *TKg*-Gal4 line, and Steve Hou for *MyoIA*-Gal4 and *Esg*-Gal4 lines; the Bloomington Stock Center, Vienna Drosophila RNAi Center (VDRC) and TRiP at Harvard Medical School for fly stocks; the Developmental Studies Hybridoma Bank (DSHB) for antibodies; Dr. Brian Gebelein for the anti-HNF4 antibody; the Biospecimen and Tissue Procurement, Redox Metabolism, and Biostatistics and Bioinformatics Shared Resource Facilities of the University of Kentucky Markey Cancer Center (supported by NCI grant P30 CA177558). This study was further supported by National Institutes of Health grants R37 AG10885 and R01 DK048498 to B.M.E.; R01 GM079684 to J.J.; U24 DK097215, R01 ES022191, P01 CA163223 and P20 GM103527 to T.W-M.F. and R.M.H; R01 HL120507 to A.J.M; R01 HL073085 and P20 GM103527 to L.A.C. Authors O.M., P.M.N. and M.O-M. are funded by the Swedish National Research Council; the Swedish Heart-Lung Foundation; Novo Nordisk Foundation; Swedish Diabetes Association; Region Skåne, ALF; and European Research Council grant StG-2011-282255. B.M.E. is also supported by the Markey Cancer Foundation. Y.Y.Z. and J.W.H. are supported by NIH postdoctoral training grants T32 CA165990 and T32 CA160003, respectively. The LC-MS/MS equipment was acquired using a National Center for Research Resources High-End Instrumentation grant (S10 RR029127 to H.Z.).

References

1. Ogden CL, Yanovski SZ, Carroll MD, Flegal KM. The epidemiology of obesity. Gastroenterology. 2007; 132:2087–2102. [PubMed: 17498505]
2. Kopelman PG. Obesity as a medical problem. Nature. 2000; 404:635–643. [PubMed: 10766250]
3. Guh DP, et al. The incidence of co-morbidities related to obesity and overweight: a systematic review and meta-analysis. BMC Public Health. 2009; 9:88. [PubMed: 19320986]
4. Polak JM, et al. Specific localisation of neurotensin to the N cell in human intestine by radioimmunoassay and immunocytochemistry. Nature. 1977; 270:183–184. [PubMed: 337160]
5. Ferris CF, Hammer RA, Leeman SE. Elevation of plasma neurotensin during lipid perfusion of rat small intestine. Peptides. 1981; 2(Suppl 2):263–266. [PubMed: 7343961]
6. Armstrong MJ, Parker MC, Ferris CF, Leeman SE. Neurotensin stimulates [3H]oleic acid translocation across rat small intestine. Am J Physiol. 1986; 251:G823–829. [PubMed: 3789148]
7. Evers BM. Neurotensin and growth of normal and neoplastic tissues. Peptides. 2006; 27:2424–2433. [PubMed: 16904238]
8. Vincent JP, Mazella J, Kitabgi P. Neurotensin and neurotensin receptors. Trends Pharmacol Sci. 1999; 20:302–309. [PubMed: 10390649]
9. Melander O, et al. Plasma proneurotensin and incidence of diabetes, cardiovascular disease, breast cancer, and mortality. JAMA. 2012; 308:1469–1475. [PubMed: 23047361]
10. Dobner PR, Fadel J, Deitemeyer N, Carraway RE, Deutch AY. Neurotensin-deficient mice show altered responses to antipsychotic drugs. Proc Natl Acad Sci U S A. 2001; 98:8048–8053. [PubMed: 11427716]
11. Piliponsky AM, et al. Neurotensin increases mortality and mast cells reduce neurotensin levels in a mouse model of sepsis. Nat Med. 2008; 14:392–398. [PubMed: 18376408]
12. Sahu A, Carraway RE, Wang YP. Evidence that neurotensin mediates the central effect of leptin on food intake in rat. Brain Res. 2001; 888:343–347. [PubMed: 11150496]
13. Boules M, et al. A novel neurotensin peptide analog given extracranially decreases food intake and weight in rodents. Brain Res. 2000; 865:35–44. [PubMed: 10814731]
14. Cooke JH, et al. Peripheral and central administration of xenin and neurotensin suppress food intake in rodents. Obesity (Silver Spring). 2009; 17:1135–1143. [PubMed: 19214175]

15. Martin S, Navarro V, Vincent JP, Mazella J. Neurotensin receptor-1 and -3 complex modulates the cellular signaling of neurotensin in the HT29 cell line. Gastroenterology. 2002; 123:1135–1143. [PubMed: 12360476]
16. Rabinowich L, et al. Sortilin deficiency improves the metabolic phenotype and reduces hepatic steatosis of mice subjected to diet-induced obesity. J Hepatol. 2015; 62:175–181. [PubMed: 25173968]
17. Lim CT, Kola B, Korbonits M. AMPK as a mediator of hormonal signalling. J Mol Endocrinol. 2010; 44:87–97. [PubMed: 19625456]
18. Xue B, Kahn BB. AMPK integrates nutrient and hormonal signals to regulate food intake and energy balance through effects in the hypothalamus and peripheral tissues. J Physiol. 2006; 574:73–83. [PubMed: 16709629]
19. Hardie DG. AMPK: positive and negative regulation, and its role in whole-body energy homeostasis. Curr Opin Cell Biol. 2014; 33C:1–7.
20. Racioppi L, Means AR. Calcium/calmodulin-dependent protein kinase kinase 2: roles in signaling and pathophysiology. J Biol Chem. 2012; 287:31658–31665. [PubMed: 22778263]
21. Shackelford DB, Shaw RJ. The LKB1-AMPK pathway: metabolism and growth control in tumour suppression. Nat Rev Cancer. 2009; 9:563–575. [PubMed: 19629071]
22. Park JH, Kwon JY. Heterogeneous expression of Drosophila gustatory receptors in enteroendocrine cells. PLoS One. 2011; 6:e29022. [PubMed: 22194978]
23. Micchelli CA, Perrimon N. Evidence that stem cells reside in the adult Drosophila midgut epithelium. Nature. 2006; 439:475–479. [PubMed: 16340959]
24. Ohlstein B, Spradling A. The adult Drosophila posterior midgut is maintained by pluripotent stem cells. Nature. 2006; 439:470–474. [PubMed: 16340960]
25. Birse RT, et al. High-fat-diet-induced obesity and heart dysfunction are regulated by the TOR pathway in Drosophila. Cell Metab. 2010; 12:533–544. [PubMed: 21035763]
26. Hewes RS, Taghert PH. Neuropeptides and neuropeptide receptors in the Drosophila melanogaster genome. Genome Res. 2001; 11:1126–1142. [PubMed: 11381038]
27. Park Y, Kim YJ, Adams ME. Identification of G protein-coupled receptors for Drosophila PRXamide peptides, CCAP, corazonin, and AKH supports a theory of ligand-receptor coevolution. Proc Natl Acad Sci U S A. 2002; 99:11423–11428. [PubMed: 12177421]
28. Song W, Veenstra JA, Perrimon N. Control of lipid metabolism by tachykinin in Drosophila. Cell Rep. 2014; 9:40–47. [PubMed: 25263556]
29. Amcheslavsky A, et al. Enteroendocrine cells support intestinal stem-cell-mediated homeostasis in Drosophila. Cell Rep. 2014; 9:32–39. [PubMed: 25263551]
30. Anderson KA, et al. Hypothalamic CaMKK2 contributes to the regulation of energy balance. Cell Metab. 2008; 7:377–388. [PubMed: 18460329]
31. Fadel J, Dobner PR, Deutch AY. Amphetamine-elicited striatal Fos expression is attenuated in neurotensin null mutant mice. Neurosci Lett. 2006; 402:97–101. [PubMed: 16632196]
32. Steinberg R, et al. SR 48692, a non-peptide neurotensin receptor antagonist differentially affects neurotensin-induced behaviour and changes in dopaminergic transmission. Neuroscience. 1994; 59:921–929. [PubMed: 8058127]
33. Fadel J, Dobner PR, Deutch AY. The neurotensin antagonist SR 48692 attenuates haloperidol-induced striatal Fos expression in the rat. Neurosci Lett. 2001; 303:17–20. [PubMed: 11297813]
34. Owens RB, Smith HS, Nelson-Rees WA, Springer EL. Epithelial cell cultures from normal and cancerous human tissues. J Natl Cancer Inst. 1976; 56:843–849. [PubMed: 176412]
35. Song J, Li J, Lulla A, Evers BM, Chung DH. Protein kinase D protects against oxidative stress-induced intestinal epithelial cell injury via Rho/ROK/PKC-delta pathway activation. Am J Physiol Cell Physiol. 2006; 290:C1469–1476. [PubMed: 16421204]
36. Li J, et al. mTORC1 inhibition increases neurotensin secretion and gene expression through activation of the MEK/ERK/c-Jun pathway in the human endocrine cell line BON. Am J Physiol Cell Physiol. 2011; 301:C213–226. [PubMed: 21508335]

37. Li J, et al. Cyclic adenosine 5′-monophosphate-stimulated neurotensin secretion is mediated through Rap1 downstream of both Epac and protein kinase A signaling pathways. Mol Endocrinol. 2007; 21:159–171. [PubMed: 17068197]
38. Yiannikouris F, et al. Adipocyte-specific deficiency of angiotensinogen decreases plasma angiotensinogen concentration and systolic blood pressure in mice. Am J Physiol Regul Integr Comp Physiol. 2012; 302:R244–251. [PubMed: 22071160]
39. Salous AK, et al. Mechanism of rapid elimination of lysophosphatidic acid and related lipids from the circulation of mice. J Lipid Res. 2013; 54:2775–2784. [PubMed: 23948545]
40. Onono F, et al. Efficient use of exogenous isoprenols for protein isoprenylation by MDA-MB-231 cells is regulated independently of the mevalonate pathway. J Biol Chem. 2013; 288:27444–27455. [PubMed: 23908355]
41. Moolenbeek C, Ruitenberg EJ. The “Swiss roll”: a simple technique for histological studies of the rodent intestine. Lab Anim. 1981; 15:57–59. [PubMed: 7022018]
42. Fan TW, Lane AN, Higashi RM, Yan J. Stable isotope resolved metabolomics of lung cancer in a SCID mouse model. Metabolomics. 2011; 7:257–269. [PubMed: 21666826]
43. Lane AN, Fan TW, Xie Z, Moseley HN, Higashi RM. Isotopomer analysis of lipid biosynthesis by high resolution mass spectrometry and NMR. Anal Chim Acta. 2009; 651:201–208. [PubMed: 19782812]
44. Palanker L, Tennessen JM, Lam G, Thummel CS. Drosophila HNF4 regulates lipid mobilization and beta-oxidation. Cell Metab. 2009; 9:228–239. [PubMed: 19254568]
45. Jia H, Liu Y, Yan W, Jia J. PP4 and PP2A regulate Hedgehog signaling by controlling Smo and Ci phosphorylation. Development. 2009; 136:307–316. [PubMed: 19088085]
46. Hipkiss AR. On why decreasing protein synthesis can increase lifespan. Mech Ageing Dev. 2007; 128:412–414. [PubMed: 17452047]
47. Stenesen D, et al. Adenosine nucleotide biosynthesis and AMPK regulate adult life span and mediate the longevity benefit of caloric restriction in flies. Cell Metab. 2013; 17:101–112. [PubMed: 23312286]
48. Alfa RW, et al. Suppression of insulin production and secretion by a decretin hormone. Cell Metab. 2015; 21:323–333. [PubMed: 25651184]
49. Park JH, Kwon JY. A systematic analysis of Drosophila gustatory receptor gene expression in abdominal neurons which project to the central nervous system. Mol Cells. 2011; 32:375–381. [PubMed: 21870111]
50. Scopelliti A, et al. Local control of intestinal stem cell homeostasis by enteroendocrine cells in the adult Drosophila midgut. Curr Biol. 2014; 24:1199–1211. [PubMed: 24814146]
51. Wang P, Hou SX. Regulation of intestinal stem cells in mammals and Drosophila. J Cell Physiol. 2010; 222:33–37. [PubMed: 19739102]
52. Jiang H, Edgar BA. EGFR signaling regulates the proliferation of Drosophila adult midgut progenitors. Development. 2009; 136:483–493. [PubMed: 19141677]
53. Gutzwiller LM, et al. Proneural and abdominal Hox inputs synergize to promote sensory organ formation in the Drosophila abdomen. Dev Biol. 2010; 348:231–243. [PubMed: 20875816]
54. Jiang K, et al. Hedgehog-regulated atypical PKC promotes phosphorylation and activation of Smoothened and Cubitus interruptus in Drosophila. Proc Natl Acad Sci U S A. 2014; 111:E4842–4850. [PubMed: 25349414]
55. Liu Y, Cao X, Jiang J, Jia J. Fused-Costal2 protein complex regulates Hedgehog-induced Smo phosphorylation and cell-surface accumulation. Genes Dev. 2007; 21:1949–1963. [PubMed: 17671093]
56. Yang L, Gal J, Chen J, Zhu H. Self-assembled FUS binds active chromatin and regulates gene transcription. Proc Natl Acad Sci U S A. 2014; 111:17809–17814. [PubMed: 25453086]
57. Reiher W, et al. Peptidomics and peptide hormone processing in the Drosophila midgut. J Proteome Res. 2011; 10:1881–1892. [PubMed: 21214272]
58. Minisymposium: The Malmo Diet and Cancer Study. J Intern Med; Design, biological bank and biomarker programme; 23 October 1991; Malmo, Sweden. 1993. p. 39-79.

59. Persson M, Berglund G, Nelson JJ, Hedblad B. Lp-PLA2 activity and mass are associated with increased incidence of ischemic stroke: a population-based cohort study from Malmo, Sweden. Atherosclerosis. 2008; 200:191–198. [PubMed: 18201705]

60. Matthews DR, et al. Homeostasis model assessment: insulin resistance and beta-cell function from fasting plasma glucose and insulin concentrations in man. Diabetologia. 1985; 28:412–419. [PubMed: 3899825]

61. Alberti KG, Zimmet P, Shaw J. Metabolic syndrome--a new world-wide definition. A Consensus Statement from the International Diabetes Federation. Diabet Med. 2006; 23:469–480. [PubMed: 16681555]

62. Ernst A, Hellmich S, Bergmann A. Proneurotensin 1–117, a stable neurotensin precursor fragment identified in human circulation. Peptides. 2006; 27:1787–1793. [PubMed: 16519961]

63. Enhorning S, et al. Plasma copeptin and the risk of diabetes mellitus. Circulation. 2010; 121:2102–2108. [PubMed: 20439785]

64. Li J, et al. PI3K p110alpha/Akt signaling negatively regulates secretion of the intestinal peptide neurotensin through interference of granule transport. Mol Endocrinol. 2012; 26:1380–1393. [PubMed: 22700584]

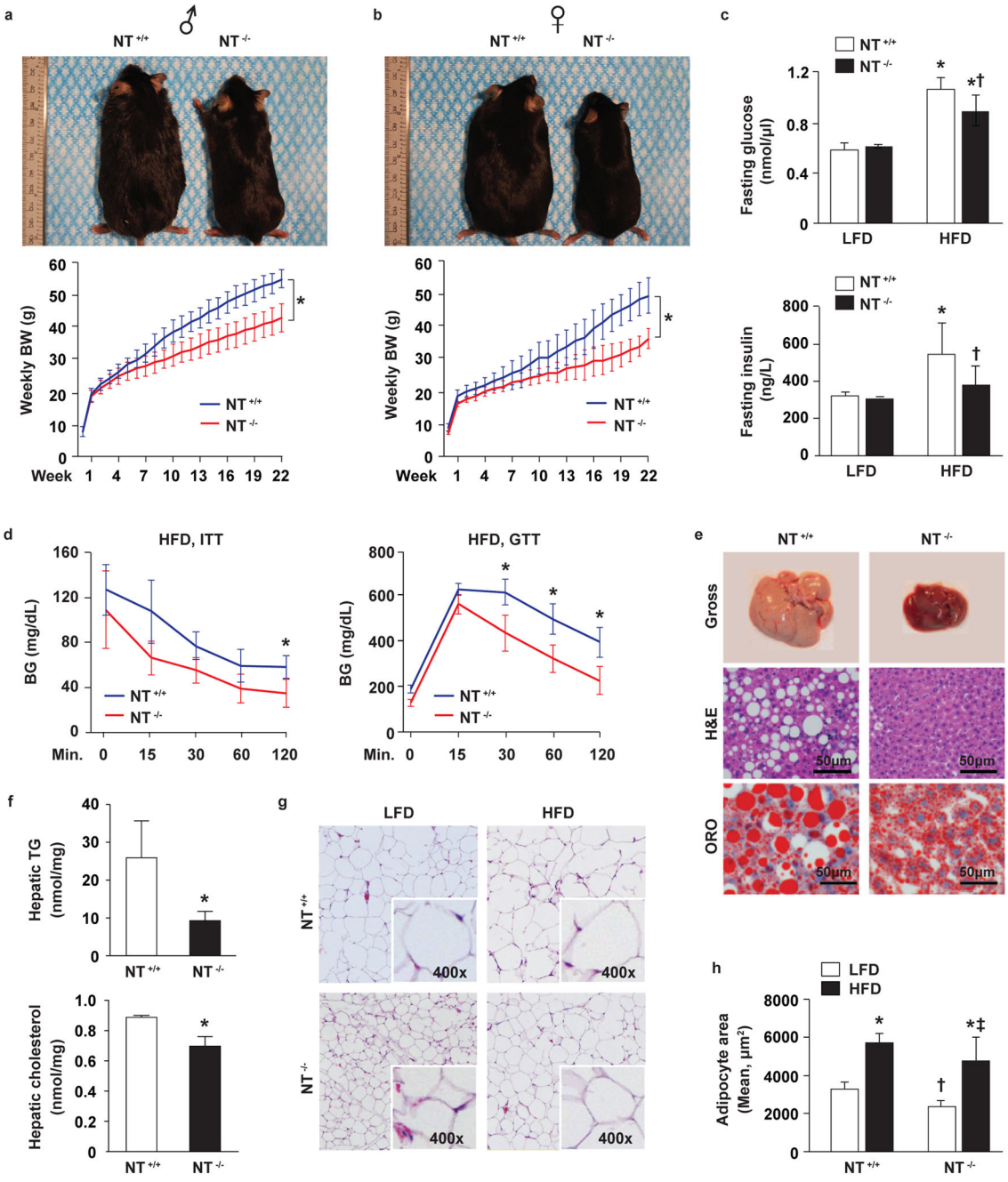

Figure 1. Protective effects of NT-deficiency on obesity and comorbid conditions

a–b. Representative male (a) and female (b) $NT^{+/+}$ and $NT^{-/-}$ mice fed a high-fat diet (HFD) for 22wks (*upper panels*). Body weight (BW) was measured weekly (*lower panels*) (male $NT^{+/+}$ n=18 and $NT^{-/-}$ n=17 mice; female $NT^{+/+}$ n=15 and $NT^{-/-}$ n=12 mice). BW slopes were compared: * $p<0.05$ $NT^{+/+}$ vs. $NT^{-/-}$ mice. **c.** Plasma glucose (*upper panel*) and insulin (*lower panel*) levels quantified in 24h-fasted male mice maintained on a LFD or HFD for 24wks (LFD $NT^{+/+}$ n=10, $NT^{-/-}$ n=10; HFD $NT^{+/+}$ n=8, $NT^{-/-}$ n=10). * $p<0.05$ vs. LFD in $NT^{+/+}$ and $NT^{-/-}$ mice, respectively; † $p<0.05$ vs. HFD in $NT^{+/+}$ mice. **d.** Blood glucose

(BG) during insulin tolerance test (ITT) (*left panel*, n=5) and glucose tolerance test (GTT) (*right panel*, n=3) in 6h-fasted male mice fed a HFD for 24wks. * $p<0.05$ vs. $NT^{-/-}$ mice. **e.** Gross, H&E and oil red O (ORO) imaging of livers of male mice fed a HFD for 24wks (n=5). Bar, 50μm. **f.** Hepatic triglyceride (TG) and cholesterol were analyzed by liquid chromatography–mass spectrometry (LC-MS) in 24h-fasted male mice fed a HFD for 24wks (n=3). * $p<0.05$ vs. $NT^{+/+}$ mice. **g.** H&E staining of epididymal fat from male $NT^{+/+}$ and $NT^{-/-}$ mice fed a LFD or HFD for 24wks (n=5). **h.** Quantitative analysis of adipocyte area (n=3). * $p<0.05$ vs. LFD in $NT^{+/+}$ and $NT^{-/-}$ mice, respectively; † $p<0.05$ vs. LFD in $NT^{+/+}$ mice; ‡ $p<0.05$ vs. HFD in $NT^{+/+}$ mice. All data are mean ± SD. Linear mixed model for a, b; ANOVA with Holm's p-value adjustment for c, h; two-sided, Student's t-test for d, f (See methods).

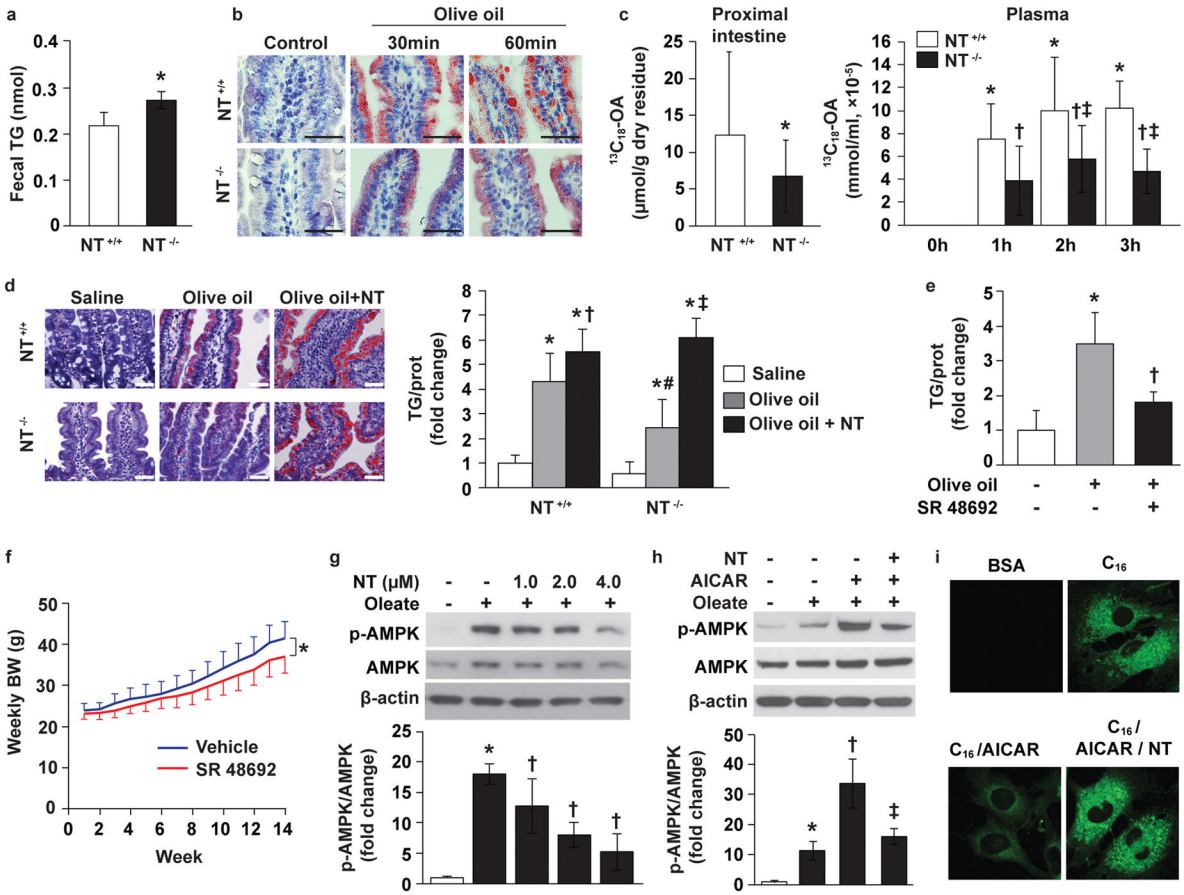

Figure 2. NT deficiency reduces intestinal lipid absorption

a. Fecal triglyceride (TG) was analyzed in male mice fed a high-fat diet (HFD) for 24wks (n=3). * p=0.05 vs. $NT^{+/+}$ mice. **b.** Oil red O (ORO) staining of proximal intestines from male mice fed normal chow with or without olive oil (OO) by oral gavage after overnight fasting (n=3). Bar, 50 **μ**m. **c.** Levels of $^{13}C_{18}$-oleic acid (OA) in male mice fed normal chow and given $^{13}C_{18}$-OA mixed in olive oil by gavage after an overnight fast were analyzed by nanospray FT-MS. *Left panel* (n=5), * p<0.05 vs. $NT^{+/+}$ mice. *Right panel* (n=4), *† p<0.05 vs. 0h in $NT^{+/+}$ and $NT^{-/-}$ mice, respectively; ‡ p<0.05 vs. 2h and 3h in $NT^{+/+}$ mice. **d.** ORO staining of proximal intestines from male mice following gavage with saline, olive oil, or olive oil plus NT (3600nmol/kg body weight, i.p.) after an overnight fast (*left panel*, n=5). Bar, 50 **μ**m; TG (in mg) was quantified in proximal intestines and normalized to the amount of protein (in mg) as described in Methods (*right panel*) (n=5). Graph presents the fold change vs. saline in $NT^{+/+}$ mice. * p<0.05 vs. saline in $NT^{+/+}$ and $NT^{-/-}$ mice, respectively; † p<0.05 vs. OO in $NT^{+/+}$ mice; ‡ p<0.05 vs. OO in $NT^{-/-}$ mice; # p<0.05 vs. OO in $NT^{+/+}$. **e.** Proximal intestines from mice given saline, OO, or OO + SR 48692 were collected and TG levels quantified as described above (n=8). Graph presents the fold change vs. control mice. * p<0.05 vs. control mice; † p<0.05 vs. mice with OO only. **f**. Weekly body weight was measured in male wild type C57BL/6 mice fed HFD and treated with SR 48692 (2.5mg/kg diluted in diH_2O and administered by oral gavage twice a day) or vehicle (vehicle n=12; SR 48692 n=13). BW slopes were compared: * p<0.05 vehicle vs. SR treatment. **g–h**.

FHs 74 Int cells were pre-treated with or without NT at different dose as indicated for 30min followed by combined treatment with oleate (0.1 mM) for 1h and western blotting of cell extracts (*top panel)*; densitometric analysis of p-AMPK is from 3 separate experiments and normalized to total AMPK; graph demonstrates the fold change of p-AMPK vs. BSA (*lower panel*). * $p<0.05$ vs. BSA; † $p<0.05$ vs. oleate alone; ‡ $p<0.05$ vs. oleate plus AICAR. **h.** FHs 74 Int cells were treated with or without NT (2 **μ**M) for 30min followed by AICAR (1 mM) for 2h and oleate (0.1 mM) for 1h and analyzed by western blot (*top panel*); p-AMPK levels were determined as in (g) from 3 separate experiments (*lower panel*). * $p<0.05$ vs. BSA; † $p<0.05$ vs. oleate alone; ‡ $p<0.05$ vs. oleate + AICAR. **i.** FHs 74 Int cells were treated with NT (2 **μ**M) for 30min followed by addition of AICAR (1 mM) for another 3h; cells were then incubated with BSA or BODIPY® FL C_{16} (C_{16}) for 15min and images taken by confocal microscopy. Representative images are from 3 experiments. All data are mean ± SD. Two-sided, Student's t-test for a, c (*left panel*); ANOVA with Holm's p-value adjustment for c (*right panel*), d (*right panel*), e, g (*lower panel*), h (*lower panel*); linear mixed model for f (See methods). (See Supplementary Fig. 1 for gel source data.)

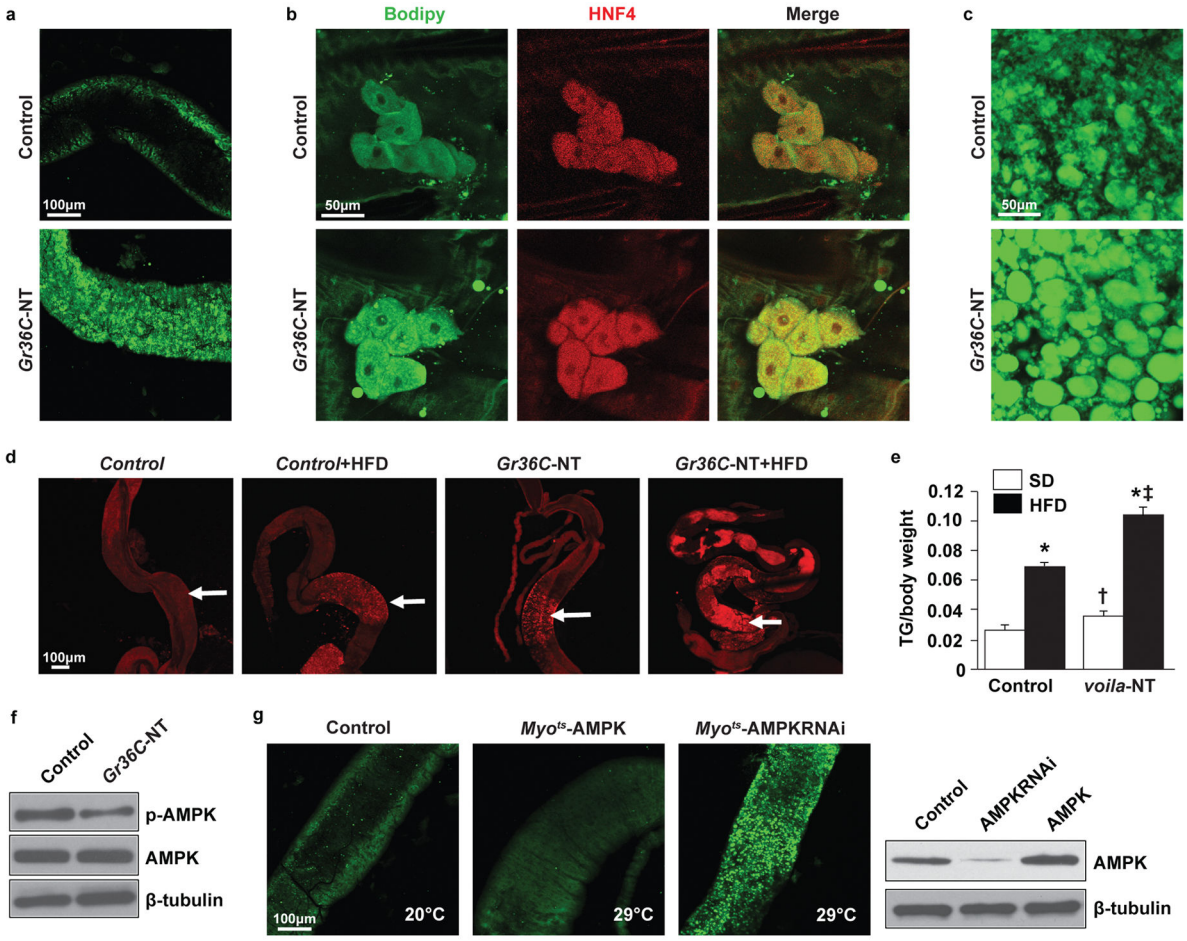

Figure 3. NT suppresses AMPK activation and promotes lipid accumulation in *Drosophila*

a. Midguts from 7d adult flies expressing either *Gr36C-w1118* (control, 100%, n=7; the percentage used here and in subsequent analyses indicates the percent of organs exhibiting the phenotype) or *Gr36C*-NT (93%, n=15) were stained with Bodipy. Bar, 100 μm. **b.** Oenocytes on the basal surface of the lateral epidermis of 3rd instar larvae expressing *Gr36C- w1118* (100%, n=15) or *Gr36C*-NT (93%, n=15) were stained with Bodipy to monitor lipid accumulation (green) and the anti-HNF4 antibody to mark the oenocytes (red). Bar, 50 μm. **c.** Fat bodies attached to the salivary gland from the 3rd instar larvae expressing *Gr36C- w1118* (100%, n=14) or *Gr36C*-NT (100%, n=8) were stained with Bodipy. Bar, 50 μm. **d.** Flies expressing *Gr36C- w1118* or *Gr36C*-NT (n=5) were treated with either standard or high-fat (HFD) diets, and guts were stained with Nile Red to examine the accumulation of lipids (arrows). Bar, 100 μm. **e.** NT was expressed by *voila*-Gal4 and TG (in mg) was measured and normalized to body weight (in mg) in male adult flies fed either standard diet (SD) or HFD (n=3). *voila-w1118* served as control. * $p<0.05$ vs. SD in control- and NT-expressing flies, respectively; † $p<0.05$ vs. SD in control flies; ‡ $p<0.05$ vs. HFD in control flies. **f.** Western blotting was performed to monitor the levels of AMPK in adult midgut shown in (a). **g.** *Myo1A*-Gal4 combined with *tub-Gal80^{ts}* (*Myo^{ts}*) does not express active Gal4 at 20°C permissive temperature. Shown in the left panel is the midgut from a 7d adult expressing *Myo^{ts}*-AMPK raised at 20°C, stained with Bodipy, and used as a control (100%,

n=11). Midguts expressing AMPK (middle panel, 94%, n=16) or AMPKRNAi^{25931} (right panel, 100%, n=12) from 7d adults at 29°C (active Gal4) were stained with Bodipy. Bar, 100 μm. The levels of AMPK were monitored by western blot. All data are mean ± SD. ANOVA with Holm's p-value adjustment for e (See methods). (See Supplementary Fig. 1 for gel source data.)

Table 1

Fasting plasma concentration of pro-neurotensin (pro-NT) in relation to obesity, insulin resistance and incidence of new-onset obesity in human subjects (Malmö Diet and Cancer Cardiovascular Cohort, MDC-CC)

	N total / N Cases	Odds ratio (95% confidence interval)				p for trend
		Pro-NT Quartile 1	Pro-NT Quartile 2	Pro-NT Quartile 3	Pro-NT Quartile 4	
Prevalent obesity	4626 / 604	1.0 (ref)	1.00 (0.78–1.29)	1.13 (0.88–1.45)	1.34 (1.05–1.70)	0.01
Prevalent abdominal obesity	4625 / 1769	1.0 (ref)	1.07 (0.90–1.27)	1.23 (1.04–1.46)	1.30 (1.09–1.54)	0.001
Prevalent insulin resistance	4468 / 1140	1.0 (ref)	1.30 (1.06–1.59)	1.43 (1.17–1.74)	1.70 (1.39–2.06)	<0.0001
New-onset obesity	2594 / 333	1.0 (ref)	1.41 (0.95–2.10)	1.79 (1.21–2.65)	2.05 (1.38–3.06)	<0.0001

N total / N cases denotes total number of subjects in the analysis divided by the number of cases with listed obesity or insulin resistance phenotype. Pro-NT Quartiles 1–4 define the MDC-CC population quartiles (lowest to highest) with median (range) baseline fasting plasma pro-NT concentrations (pmol/L) of 60.1 (3.3–75.9), 89.3 (75.9–105), 123 (105–149) and 190 (149–1155), respectively. Data are presented as odds ratios (95% confidence intervals), and subjects belonging to the lowest quartile of pro-NT were defined as the reference group (odds ratio =1). p for trend denotes the p-value for linear trend over quartiles 1–4. Logistic regression models were used for comparisons between quartiles and linear trends over quartiles (see Methods).